REAL-TIME OPTIMAL CONTROL OF LARGE SCALE POWER SYSTEMS WITH APPLICATION TO IMPROVING TRANSIENT STABILITY RESPONSE

By

GREGARY C. ZWEIGLE

A dissertation submitted in partial fulfillment of
the requirements for the degree of

DOCTOR OF PHILOSOPHY

WASHINGTON STATE UNIVERSITY
School of Electrical Engineering and Computer Science

MAY 2013

To the Faculty of Washington State University:

The members of the Committee appointed to examine the dissertation of GREGARY C. ZWEIGLE find it satisfactory and recommend that it be accepted.

_____

Vaithianathan Venkatasubramanian, Ph.D., Chair

_____

Anjan Bose, Ph.D.

_____

Mano Manoranjan, Ph.D.

ACKNOWLEDGEMENT

Don Wiseman, my good friend, diagnosed with cancer, provided my initial motivation to renew chemistry and physics studies, then broaden my engineering skills. I wanted to better understand the important challenges facing our world and improve my ability to contribute solutions. Curiosity draws me to science and creating to engineering. But seeing good, what is needed, and making a contribution to society, even small, drives me.

Washington State University supported my part-time student role both for this PhD and a recent MS (Physical) Chemistry degree. I appreciate the professors who helped me learn many new things now and during previous degrees at Northwest Nazarene University (BS Physics) and WSU (MS EE).

Schweitzer Engineering Laboratories, Inc. encouraged my studies and funded them. Every day SEL provides an environment where I can contribute towards improving electric power systems, so critical to modern life.

My family continues to tolerate me reading textbooks. I appreciate their patience.

REAL-TIME OPTIMAL CONTROL OF LARGE SCALE POWER SYSTEMS WITH APPLICATION TO IMPROVING TRANSIENT STABILITY RESPONSE

Abstract

By Gregary C. Zweigle, Ph.D.
Washington State University
May 2013

Chair: Vaithianathan Venkatasubramanian

Electric power systems are large nonlinear dynamical systems and therefore require unique control designs compared to the linear systems engineers often encounter. A special characteristic of the power system is structural change as a control option, with end-point stability the objective. However, these structural changes are not always treated rigorously when control systems are designed today. This research investigates the theory of control through structural changes and shows the need for an optimality based approach. A control framework is then created that considers both state trajectory and control action performance measures. Recovery to a stable operating point is through rapid and minimal control actions, which simultaneously are selected to constrain the dynamic response of relevant state variables along the path towards stability. The approach is well suited for responding to high order contingencies. These contingencies, while rare, are difficult to mitigate with existing controls, and can lead to cascading system collapse.

Subsequently, several realizations are researched, designed, analyzed, and validated. The first is a solution that places few constraints on implementation complexity. It is model-based and predictive for control selection. Then, an improvement is developed that decreases computational requirements by reducing the space of admissible controls. A method to select this space that exhibits minimal impact on system disturbance response is invented. Finally, the optimality constraint is relaxed, but in a manner that maintains much of its original benefits. No model is required. Each of these instances demonstrate robustness to parameter errors, robustness to control actuation failures, robustness to modeling errors, and a significant improvement in the disturbance size the controller can tolerate while driving the system to an acceptable solution, compared to present approaches. Performance trade-offs between optimality of the selected controls and computational demands of the controllers are investigated. Experimental validation of results is demonstrated with the IEEE 39-bus test system.

TABLE OF CONTENTS

LIST OF TABLES

LIST OF FIGURES

1.0 INTRODUCTION

This chapter summarizes the dissertation motivation. Existing literature is surveyed. An overview of the dissertation research is provided along with a summary of key contributions.

1.1 Motivation

The electric power system provides critical infrastructure for society and it must maintain a specified level of performance even during severe unexpected disturbances. The system is also very large, highly nonlinear, and with time varying characteristics. Furthermore, it exhibits the unique feature of structural changes as the initiating disturbance and often the disturbance response. This is in contrast to most controlled systems cast as a time signal arrangement. The engineering challenge to meet required performance is simultaneously difficult and interesting.

Consider the problem of designing a system with synchronized power generating and receiving devices, spread over thousands of kilometers, and interconnected with a mesh network carrying all power exchanges. Although rotating in isolation, generators are electrically coupled. Power consumers continuously switch in and out of service. The demand quantity and electrical characteristics of loads are never constant. Power flows in the system are very large, with individual generation stations capable of delivering on the order of 1,000 megawatts (approximately 1,300,000 horsepower) of power and the total capacity in the

United States alone near 1,000,000 megawatts (1 terawatt). The dynamics of every device is intertwined with all of the other machines and devices in the system through a network of connections, and that network itself varies in both topology and electrical capability. All of these dynamics are nonlinear in nature. The electric power system is perhaps the largest, most complicated man-made machine ever created and is considered one of the great engineering achievements of modern time [1].

The nonlinear nature of the electric power system deserves special attention. Well-developed mathematical theory and analysis exist for linear systems and nearly all commonly known areas of science and engineering are approximated as linear. Electromagnetic radiation described by Maxwell's equations follows linear relationships and, although complicated, at least the mathematics of quantum mechanics is linear. For linear systems the whole is exactly the sum of the parts. Decomposition into constituent pieces is allowed, as is individual analysis, and subsequent reconstruction into mathematically tractable and understandable explanations makes problem solutions neat and organized.

In contrast, with nonlinearities, even the simplest systems become impossible to solve almost immediately [2]. John Guckenheimer has written, "We must start by admitting that almost nothing beyond general statements can be made about most nonlinear systems" [3]. The practical unpredictability of chaotic behavior emerges starting with only three time-invariant nonlinear differential equations. Now consider that the electric power system consists of not three nonlinear differential equations, but at least hundreds or thousands of nonlinear differential equations [4]. So, the challenge for the power engineer is to design and maintain a system that is critical to modern society and must operate with near perfection,

while simultaneously the system is mathematically described at a level where the theory is exceptionally challenging.

One strategy that helps avoid nonlinear complexities and aids in reliable power system operation is keeping the system near its equilibrium point. During normal operation, generator rotors rotate in synchronism and their relative angles maintain slowly varying relationships. Also, power flows remain steady. The voltages and currents in the system stay within well-understood ranges. Oscillations are small and under control. Equilibrium operation allows linearization of the system both for analysis and design of controllers. As long as the power system operates in historically consistent ranges then unreliable behavior is avoided and this is the case most of the time.

However, the electric power system does not operate in isolation. It is subject to a variety of external events that are often very significant, such as severe weather, structural failures, and, more recently, the stochastic nature of renewable generation sources. When the system suddenly demands an excessive change in energy, rotors can experience large excursions, even to the point of swinging outside of their normal equilibrium relationship. Special care is required to keep the system stable during these excursions. Systems that tolerate disturbances while maintaining stability enable safe, high energy transfer over existing transmission lines, and, especially important today, enable increasing the penetration of new generation sources such as wind and solar.

Hierarchies of protection and control are employed to ensure reliable operation when the system moves too far from its equilibrium state. The lowest level of defense is local protection, which disconnects selected components of the system after detecting faulted

conditions. Protection at this level utilizes localized signals to make decisions, and is responsible to control local network sections. At the highest defense level, system operators monitor and control wide sections of the power system. During a disturbance, operators are often confronted with complex situations and must make difficult decisions in relatively short time-spans.

For some potential disturbances, the required breadth of decision making information exceeds what is available at the local level and the maximum time allowed to make the correct decision is less than what is humanly possible at the operational level. In these cases, system integrity protection systems (SIPS), also sometimes called remedial actions schemes (RAS), collect wide-area information and make automated decisions with the intent of preserving the system and keeping performance within acceptable limitations. The integrity of the system is equated with a stable disturbance response and acceptable performance limits are equated with important states remaining within specified ranges.

Power system stability theory is divided into several classifications, to reflect the different physical cause of instability modes, the different size of disturbances, and to make clear relevant time-spans, devices, and processes involved [5]. Voltage stability relates to the ability of the system to maintain system voltages within certain limits. The electric power system today is designed such that power is controlled through current variations while voltage is held constant. Declining voltage violates design assumptions resulting in an increase in current to maintain the power draw, which can act as a positive feedback driver to further push voltage lower until the system collapses. Frequency stability relates to the ability of the system to balance power delivery and power demand. Rotor angle stability, also known

as transient stability, is a class specific to the electromechanical nature of most generators driving the electric power system. When rotors are unstable they swing through extra cycles. This disrupts generated power, can damage equipment, and lead to other forms of instability.

Good system planning, including well designed local protection and SIPS help prevent instability. These approaches result in very reliable systems by identifying contingencies that lead to instability and designing solutions for each individually. However, it is not always possible to plan for every contingency. Typical expectations are stability for all single, denoted (N-1), and sometimes credible double, denoted (N-2), contingency failures. In a system with N lines there are N possible single line failures and $\binom{N}{2}$ possible double line failures. Electric power systems are characterized by large numbers of connections and it is not always practical to consider additional failures cases, with $\binom{N}{k}$; $k > 2$ possible permutations. For example, a minimal version of the New England power system includes 46 connections, resulting in 2^{46}, or over four trillion possible line outage combinations. This number is further increased when other failure modes besides transmission lines, such as stuck breakers, are included in the considered contingency set.

Fortunately, as k increases, the probability of a given contingency occurring rapidly decreases. Given equally likely and independent statistics, the probability of k simultaneous line outages is p^k,where p is the probability of a single line outage. Often it is appropriate to neglect all k > 2 cases. And yet, because electric power is very important in today's high technology world, systems and methodologies able to tolerate rare, difficult to predict events

are worth investigating. Larger-order transmission contingencies decrease overall reliability and increase the risk associated with them [6][7].

In addition to the large possible failure space, another challenge for system reliability during SIPS design is model accuracy. Ability to distinguish stable from unstable system responses is a function of model parameter accuracy and model structure. For preplanned controls, the model parameters are effectively fixed by the time the system is put into service. Parameter uncertainty may force the preplanned scheme into more conservative responses than minimally necessary. For example, shedding extra generation or load in order to reach a satisfactory guarantee the resulting system configuration is stable.

The electric power industry needs continued innovation in the area of control methods for large nonlinear systems that help improve reliability. Advancements in theory and design are required. This dissertation contributes to both.

1.2 State of the Art

The first step in controlling something is measuring it. Unfortunately, the physical size of the electrical power system makes a measurement of its state difficult. For example, consider the challenge of measuring the voltages and currents at every bus. There might be thousands of substations, each separated by hundreds of miles. Historically this impeded development of wide-area feedback-based control schemes because accurate state measurements, or, at least, good estimates, are required. Time-synchronized phasors, also known as synchrophasors, utilize a global timing signal to place a precise time-stamp on each

network measurement. This measurement approach was initially proposed in the 1980's [8], with further theoretical development in the 1990's [9]. Deployment of the Global Positioning System [10] provided a convenient source of the timing signal. During the decade of the 2000's phasor measurement units (PMU), devices that measure the power system network state with a precise time-stamp, became available at low cost [11][12] and deployed for many applications [13]. These advancements enable fast, high quality, and time-aligned measurements of the power system network state.

For the innovation developed in this dissertation, knowledge of system machine states is also necessary. A relatively recent advance in the area of time-synchronized measurements is in the measurement of electrical machine rotor angle [14][15]. Also, research results are appearing for measuring other electrical machine state variables such as excitation signals [16]. Time-synchronized measurement of the network state and the machine state are foundational technologies for the research in this dissertation. They provide the measurements which make new wide-area control methods possible.

Two other technology advancement which make new control methods possible are fast reliable communication networks [17] and high speed computing. Delay in control actions is almost always destabilizing to feed-back controller performance. Processing time to calculate decisions results in delay and for wide-area systems the communication network latency directly counts towards control loop delay. This dissertation is not intending to solve all of the various implementation issues but it is helpful that continuous advancements in these areas make approach such as the ones developed in this dissertation more implementable.

The most common methods today for wide-area system integrity protection are offline planning with look-up tables [18], as mentioned in the previous section, and direct energy function methods [19] including the equal area criterion [20]. The preplanned methods are very fast because they sense topology changes, which often precede signal changes. But they have limited adaptability to changing system topology and state, are susceptible to modeling and parameter errors, and do not provide a framework to move functionality from saving the system, a protection operation, to controlling the system such that the protection operation is either no longer necessary or becomes an even more rare event. Feedback control with synchrophasors and a voltage magnitude measuring system have been developed as well [21].

An emerging control approach for nonlinear systems is finite horizon, model based prediction. Model based prediction control was originally formulated for complex control applications such as chemical processing [22]. It has been applied to electric power for control of voltage related stability [23][24][25]. The single machine equivalent method includes prediction in a transient stability control scheme along with an optimality approach for generator control [26][27][28]. Relating to transient stability prediction, a real-time simulation approach for stability assessment through prediction has been developed [29]. Rotor angle stability prediction has been investigated [30][31], as assessment, which is a first step for subsequent control. Applications with model predictive control to damp small and large signal oscillations [32][33] have been reported.

1.3 Formulation

Power systems often apply structural changes as control and yet fundamental theories of this approach are immature. Therefore, a theoretical framework is developed in this dissertation. A key result of this new theory is showing that an optimal formalization is necessary to properly selected between competing viable structures. Also, a new class of control instability is identified. The driving forces of control instability are analyzed.

The present research then applies this new theory to design a feedback controller that reflects the full nonlinear nature of the system which it controls, and finds a solution optimal in the sense of minimizing state trajectory and actuation costs. The design is feedback iterative for robustness and built for real-time implementation. Realizations include both model driven with prediction controllers as well as a model-free with buffered measurement controller. The research includes both theory and analysis in coordination with the design.

The resulting solutions are shown to provide several benefits. They stabilize higher order contingencies than preplanned schemes are capable. Costs are included in decisions. States are tracked and controlled over the full transient trajectory. The iterative, feedback nature of the controllers improve robustness to modeling errors and state initialization errors. Such feedback also increases robustness to actuation failures. Application of either short-window prediction or historical measurements, both with feedback, mitigates some of the nonlinearity challenges because the response adapts to conditions outside of the forecast. The controllers can respond therefore to unanticipated events. The system captures complex levels of modeling detail in control selection, unlike approaches such as equal area [20]. Finally,

these controllers are shown to exhibit good performance even with limitations in control options and with system feedback delays due to communication latencies.

The developed method is applied specifically in this dissertation to correct transient instabilities. This provides a tangible environment for explaining the concepts. However, the framework and control methods developed also apply to correcting other types of instability, when the control response is through structural changes in the system. Rotor angles for a transiently unstable power system experience large deviations and this can lead to generation falling out-of-step with the rest of the system. A benefit of the new controllers is correcting this condition through structural changes prior to the system separating in an uncontrolled manner.

An important constraint on real-time control for transient stability is response time. The initial feedback controller developed in this dissertation requires significant computations. This is because of its optimal theory based approach, which can suffer from a "curse of dimensionality" [34]. Methods exist to improve computational performance [35][36] but are not easily applicable to the system designed here because of its nonlinear nature and the method of control through structural changes. Therefore, simplifications to the controller are designed. A classification algorithm is developed which reduces the space of admissible controls in a manner that does not prune structures which lead to an acceptable cost result. Then, a model free solution is designed which requires only historical state measurements. Controllers developed following the principles of both are shown to successfully stabilize transiently unstable systems. However, the trade-off is a less optimal control selection. Also, the applicable space of unstable systems is reduced. These results are shown experimentally.

1.4 Contributions of the Dissertation

1. A new framework for controller design that acts through structural changes and dimensional reduction is proposed.
2. It is demonstrated why applying structural changes as control requires a cost-based approach [37].
3. A form of instability due to excessive control actions is identified [37].
4. Optimal control for large signal transient stabilization, using discrete dimensional reduction as the control method, is developed and analyzed [38] [15]. The algorithm is designed along with experimental validation [37]. Somewhat related, the requirements of real-time control to the communication network is examined [17].
5. A classification method that reduces the computational demands of the controller is designed, analyzed, and demonstrated experimentally [39].
6. A model free historical measurement based controller is designed, analyzed, and demonstrated experimentally [40].

2.0 THEORETICAL FRAMEWORK

This chapter develops a framework relating to systems which control through discrete structural changes, including dimensional reduction. Electric power systems have long allowed structural changes as control actions. However, what is needed is a design methodology that formalizes this approach and can provide the foundation for new control solutions.

2.1 Foundation

Consideration is given to differential equations with the form specified as follows.

$$\dot{\underline{x}} = \underline{f}_d(\underline{x}) \qquad 2.1.1$$

The vector $\underline{x} \subset \mathbb{R}^{n(d)}$ is the system state, and $n(d = 0) = \mathcal{N}$. The $\underline{f}_d(\cdot)$ is a nonlinear vector field, and each structure index d is for a different system. The theory places no constraints as to how the systems relate to each other.

Control is through discrete changes in the structure of the system, indicated by d_k, which allows the progression of time through index k. No signal based controls are considered. If a continuously acting control is needed, then it is incorporated into the method through quantization and then including as a separate structure. This is in contrast to a more

typical control system, of the form $\underline{\dot{x}} = \underline{f}(\underline{x}, \underline{u})$, where $\underline{u}$ is a control acting in a time-series manner as a signal input to the system.

The method of control developed here is unusual for control theory, but not unusual for power systems. Consider load shedding. This is a discrete structural change that, at most, eliminates a set of differential equations from the system, or, at least, step-changes the existing differential equations. If any differential equations are eliminated, it is identified as control through dimensional reduction. Then, the system is allowed to evolve along a path as determined by whatever existing dynamics and controls are in place. The fact that existing controls are left to drive the system according to their pre-designed nature is an important concept. This research does not seek to actively modulate existing closed-loop controls. Instead, it step-changes the structure of the system, with the goal of allowing existing controls to take the system towards an equilibrium point of their design.

A simple example gives some insight into the range of structure index d. Consider the case where each set of state collections corresponds to a unique structure and no other structures are available to the system. In this case $d \in \left\{0, 1, 2, \dots, \sum_{i=0}^{\mathcal{N}} \binom{\mathcal{N}}{i} = 0,1,2, \dots, 2^{\mathcal{N}} - 1\right\}$, which represents all possible combinations of states. If there are initially three state variables, $\mathcal{N} = 3$, then $d = 0$ is associated with a state vector that includes all three states. Subsequently, $d = 1$ is associated with a state vector that includes, for example, states $\{x1, x2\}$; $d = 2$ is associated with a state vector that includes states $\{x1, x3\}$; $d = 3$ is associated with a state vector that includes states $\{x2, x3\}$; $d = 4,5,6$ are associated with state

vectors that include single states $\{x1\},\{x2\},\{x3\}$; and $d = 7$ is for a null system, with no states.

In general there are multiple structures available for a given set of states. Given the previous example, perhaps five structures exist for a system composed of states {1,3}. The result is five sets of two differential equations. Therefore, the range of the structure index d is $d \in \{0,..,D\}$ where each value is not necessarily associated with any specific dimension of the system, and where D is system dependent. The only constraint is that $d = 0$ is the starting system and has dimension $\mathcal{N}$.

Control Objective

The objective is to design a sequence $\{d_k\}, k = 0, \ldots, K$ such that

1. $\underline{x}(k)$ is transferred from its initial state to a target region X.

$$\mathrm{X} = \{\underline{x} | r(\underline{x}) = \underline{0}\} \qquad 2.1.2$$

2. A performance measure, or, cost, is minimized along the trajectory to X.

$$\mathcal{J} \equiv C(\underline{x}_k, d_k) \qquad 2.1.3$$

Constraints

The solution is subject to four constraints.

1. Equation 2.1.1.

2. $d_k \in \mathcal{D} = \{d | g(d) = 0\}$. This is the set of admissible structures, as selected by admissible controls. There is a slight difference between admissible structures and admissible controls. The controls are actions that take the system from one structure to another. Because admissible structures and admissible controls are closely related the terminology is used interchangeably when the distinction is immaterial. In a typical control system, the admissible controls are in terms of signal ranges and signals meeting limits. In the case considered here, when control is through a series of structural changes, the admissibility constraint is because of the requirement to remain with a subset of the set of all possible structures. Considering the load shedding example, there are often loads that are not available for removal because of their importance. Another example is a dynamic brake located at a specific bus. A controller calling for dynamic brake insertion at a location where not installed is disallowed.

3. Structures cannot repeat as the result of a control action, unless a subsequent structural change has restored the original structure. Once a load is removed from the system, the controller cannot remove that load again. Similarly, if a generator is removed from the system, or, if spinning reserve generation is added to the system, it is meaningless to try removing or adding it again. An example of allowing a repeated

change is if a generator is removed from service and later is placed back into service. In this case the original removal action is allowed to repeat.

4. Consider exclusively structures and controls which depend on the present or previous states and the previous history of controls.

2.2. Structural Changes and Equilibrium

A structural change is visualized as shown in Fig. 2.2.1. The phase portrait on the left is a representation of the initial dynamical system, with vector field $\underline{f}_{d_{k-1}}(\cdot)$. The control action transforms the vector field $\underline{f}_{d_{k-1}}(\cdot)$ to $\underline{f}_{d_k}(\cdot)$, as shown on the right, and the state $\underline{x}_{k-1}$ in system on the left is transferred to state $\underline{x}_k$. Transferring to the new system can involve eliminating a set of states as a form of dimensional reduction driven control. At the instant after transformation, states in the new system have identical values to their corresponding initial state values in the original system. In the course of this reduction, parameters in the new space can change. Historically, the hope has been that the new dynamical system contains stable equilibrium points and that the initial state $\underline{x}_k$ is within a domain of attraction of a stable equilibrium point in the new system. In contrast, the method developed here provides a framework to design a system that achieves this objective.

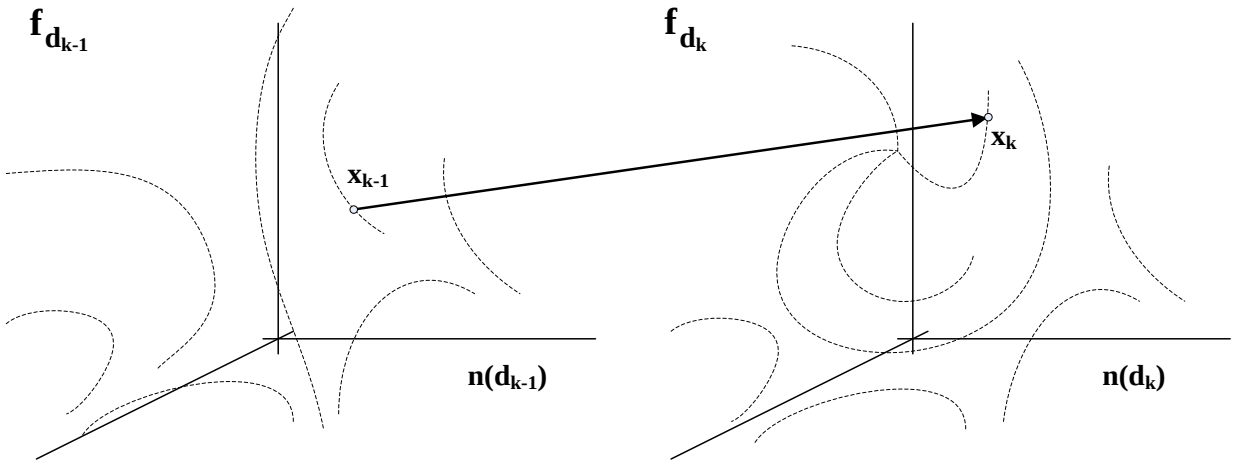

Figure 2.2.1. Phase portrait (stylized) response to control.

Again, control through structural change is not a method of actively guiding the state along a trajectory towards a stable equilibrium point. Instead, this is a discrete control method that relies on existing control schemes to provide that transfer. The role of structural change is to modify the composition of the phase portrait such that within this new dynamical system the initial state is in the region of attraction of a valid stable equilibrium point. One way this can happen is when the location of equilibrium points, the number of equilibrium points, and the stability characteristics of these points remain the same in $\underline{f}_{d_{k-1}}(\cdot)$ and $\underline{f}_{d_k}(\cdot)$. When the state is projected into the new space, $\underline{f}_{d_k}(\cdot)$, it becomes within the domain of attraction of an equilibrium point and is transferred to that point by the dynamics of the new system. Another possibility is when the nature of equilibrium in $\underline{f}_{d_{k-1}}(\cdot)$ and $\underline{f}_{d_k}(\cdot)$ are different, and in the new space the mapped state is within the domain of attraction of a stable equilibrium point.

Consider a simple nonlinear dynamical system, Eqn. 2.2.1 [41]. The phase portrait is shown in Fig. 2.1.2 with $\alpha = 1$ and $\beta = 2$. This system is defined by vector field $\underline{f_0}\left(\begin{bmatrix} x \\ y \end{bmatrix}\right)$.

$$\begin{aligned} \dot{x} &= \alpha(\beta^2 - x^2) \\ \dot{y} &= -\beta^3 y \end{aligned} \qquad 2.2.1$$

There are two fixed points in this system, one at $\{x, y\} = \{-2,0\}$ and one at $\{x, y\} = \{2,0\}$. The first equilibrium location is a saddle-point and the second is a stable node. Stability of any given instance of this system depends on its initial conditions. The initial state $\{x, y\} = \{-3,0.6\}$ leads to instability because the state variable x increases without bound. This point is shown by the dark circle in the upper left corner of Fig. 2.2.2.

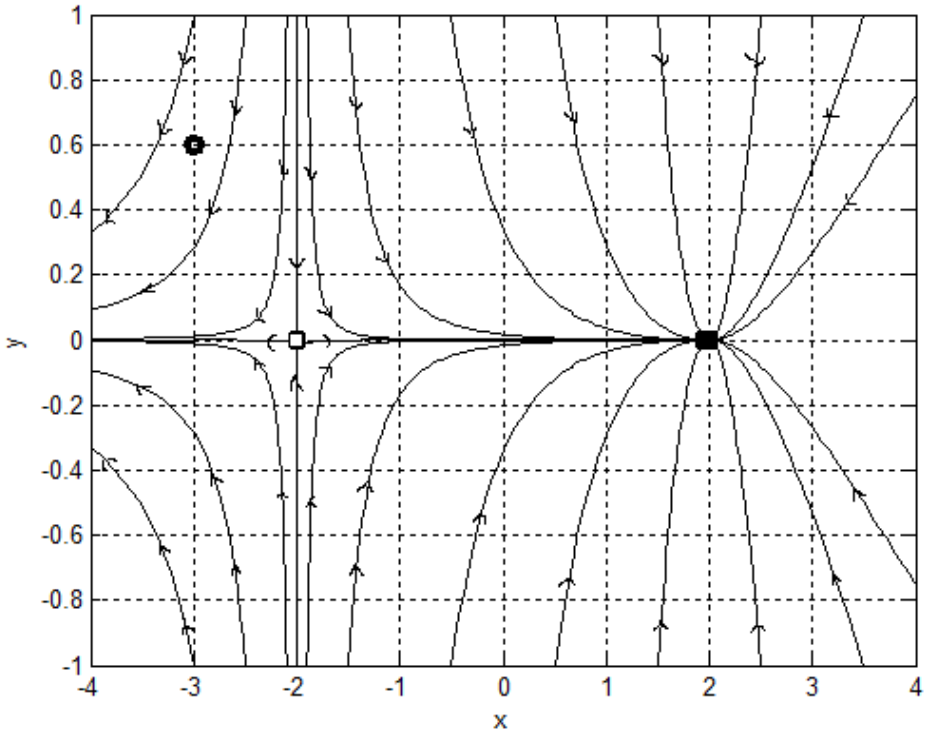

Figure 2.2.2. Phase portrait for first example.

Setting $\alpha = 0$ eliminates state variable x, and reduces the dimension of the system by one. The new dynamical system is defined as $\underline{f_1}(y)$. This is an example of controlling the system by dimensional reduction. The new system is globally stable. However, the dynamical equation $\dot{y} = -\beta^3 y$ has no changes to the value of the equilibrium point for y. Notice in Fig. 2.2.2 that state y always converges towards an equilibrium $y = 0$, even when state $x \to -\infty$.

A modification to Eqn. 2.2.1 provides an example of the case when dimensional reduction changes the nature of an equilibrium point for y. The vector field is $\underline{f_2}\left(\begin{bmatrix} x \\ y \end{bmatrix}\right)$.

$$\begin{aligned} \dot{x} &= \alpha(\beta^2 - x^2) \\ \dot{y} &= -\beta^3 y - \alpha\beta x \end{aligned} \qquad 2.2.2$$

The phase portrait for Eqn. 2.2.2 with the consistent values of α and β is shown in Fig. 2.2.3. There are two fixed points in this system, one at $\{x, y\} = \{-2, -0.5\}$ and one at $\{x, y\} = \{2, 0.5\}$. The first equilibrium location is a saddle-point and the second is a stable node. Setting $\alpha = 0$ again eliminates state variable x, and reduces the dimension of the system by one, now defined as $\underline{f_3}(y)$. The new system is stable. However, unlike the previous example, in this case, the equilibrium points for y change. Setting $\beta = 0$ and keeping α at its original value shows the opposite case, where the new system is not stable.

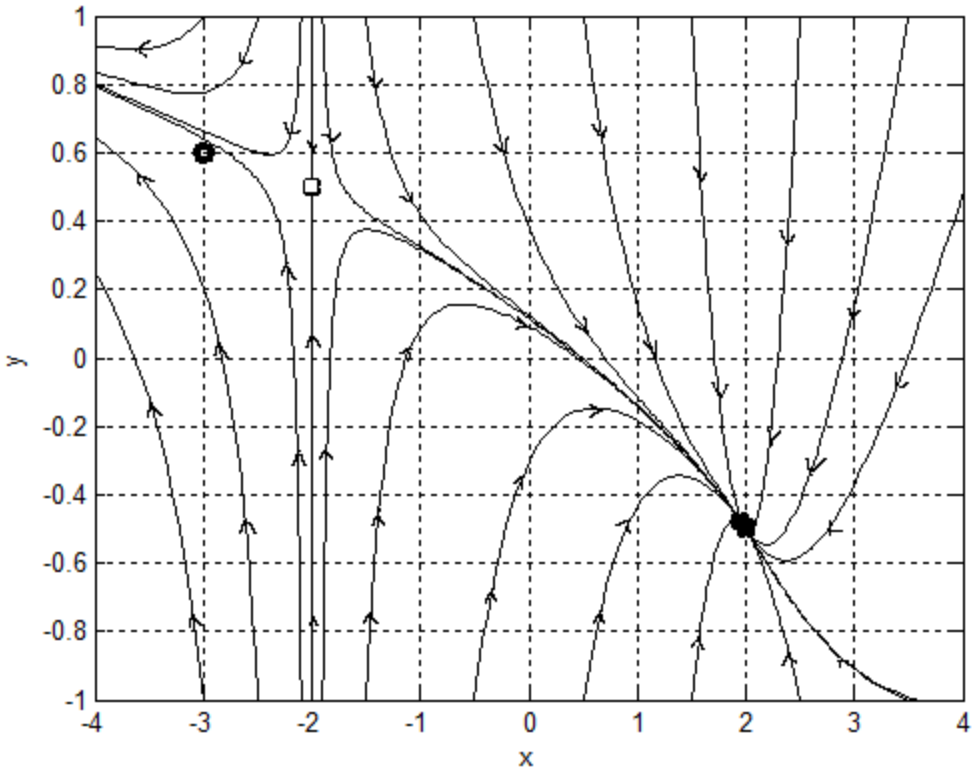

Figure 2.2.3. Phase portrait for second example.

These examples have demonstrated various cases for what can happen to equilibrium locations after structural changes. The responsibility of the controller is to select the correct sequence of structures, which may include dimensional reduction, such that the new dynamics transfer the initial state to the target region X, and do so in a manner that meets performance objectives.

2.3 Controllability

The present method builds on a power system characteristic of structural system changes as both the initiating force of instability and an available control actuation mechanism to recover. Implementing control as a step change in system structure is not a typical approach outside of the electric power industry. Figure 2.3.1 illustrates a common control system architecture. The controller drives the system G with a signal input. The controller does not change the structure of the system G. However, in electric power systems actions like generator tripping, line tripping, series compensation, and load shedding are structural changes to the system G.

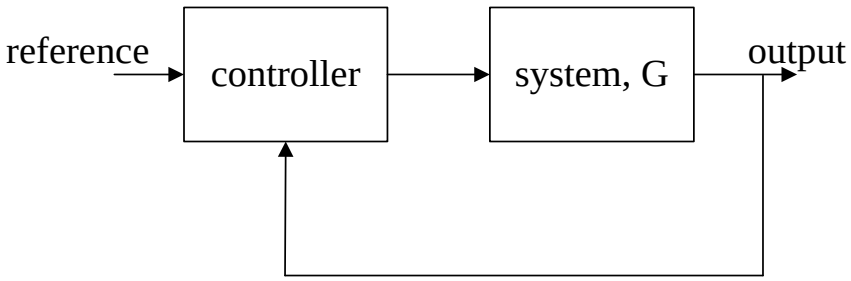

Figure 2.3.1. Typical control system block diagram.

Often when electric power is stabilized with emergency controls the primary objective is stabilization. However, with full freedom to change G it is apparent that stabilizing any contingency is possible, and from any post-contingency initial state. This is true as long as states removed through dimensional reduction are defined as included in target region X, per Eqn. 2.1.2. For example, removal of unstable states as is done when tripping a generator is a structural change. In this case, if the remaining system is transferred to a stable equilibrium point, then the control action is considered successful. It is acceptable that the state variables

associated with the generator are removed from the system and, by definition, their values are included in X. The perhaps surprising conclusion is that if stability is always achievable then the design focus shifts from merely stabilizing the system, towards stabilizing the system at minimum cost.

An initial state $\underline{x_o}$ of a control system is defined as controllable if a set of admissible controls $\{d_k\}$ are available that can transfer the state to the target X in finite time. The set of all initial states that are controllable is called the controllable set [35]. If the initial states are held at the target then, in a broad usage sense, the system is stable for those initial states. The domain of attraction is the set of initial states that are taken to the target region [35]. Because the control system developed here works through structural changes, and then allows the system to evolve under its existing control mechanisms, there is really no way to guarantee that the system reaches its target asymptotically. Furthermore, such a characteristic is not important for this application. As long as the system is taken from instability, to a point in a new structure where it is within the domain of attraction of X, then time and resources become available to the existing controls to finish the task of bringing the system to its final desired state.

If the set of admissible controls includes the ability to switch all sources and loads, then one of the available responses for a large contingency is to completely disassemble the electric power system, removing all generation and all loads. The system is at a target X because of the allowance to dimensionally reduce the system. The problem with this approach is that the cost of these control actions is not considered. Removing generation involves eliminating a revenue source. Removing load involves disconnecting people from

infrastructure that is critical to modern life. This simple example demonstrates why it is only possible to design control based on structural changes if the cost of controls are included in the design. However, this is not always the method applied today when designing controls for electric power systems that include structural changes. Additionally, it is desired that electric power states remain within certain limits, even during transient evolution towards a stable and acceptable equilibrium point. So, cost of state deviation from an acceptable path is also important to measure. This dissertation shows how to include control and state deviation costs in a controller based on structural changes.

Excessive disassembly of the system is a form of control driven instability, defined later. For example, during the 2003 East Coast blackout some lines were opened, as designed, because large signal excursions were detected [42]. The system eventually settled to a stable equilibrium point and if stability was the only measure, then the resulting configuration should be considered successful. But it is widely agreed that the cost to bring the system to its final state was excessive. A less expensive solution was possible if the controls acted different. It was the existing controls themselves that drove the system to an unacceptable state, implying that stability analysis and control without considering in-place controls is not always useful.

2.4 The Cost Metric

The task of developing an appropriate cost metric starts with a specific example. Consider the Kundur 2-area system, as shown in Fig. 2.4.1. This system is modified by the doubling of each generator, with the purpose of providing extra granularity in considering various control options. Each generator is set to deliver one unit of power. The loads are arranged so that the power draw at bus #12 is six times the power draw at bus #10. Therefore, significant power is flowing from left to right, through line 10-11.

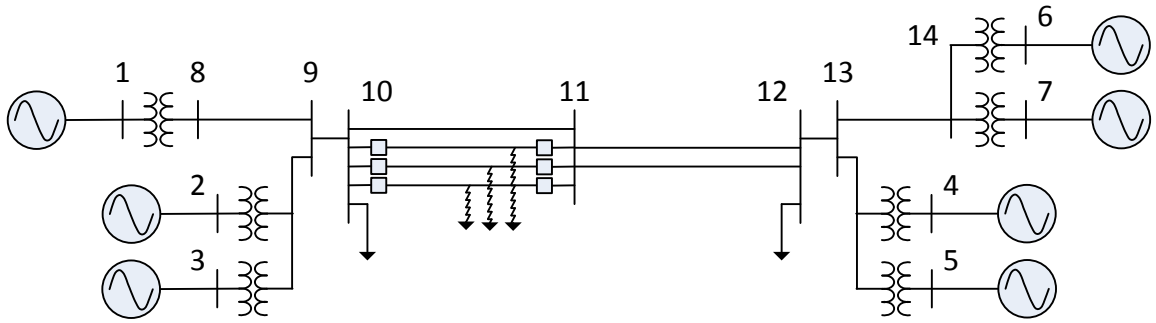

Figure 2.4.1. Kundur 2-area system.

Because this dissertation is particularly interested in higher order contingencies, the case where three of the four lines connecting bus #10 to bus #11 fault and then disconnect from service is investigated. The fault is set to persist on the line for 500 milliseconds prior to tripping. The result is a significant accelerating power at each generator. The initial system is defined as $\underline{f}_0(\cdot)$. During the fault, the system is given by a new set of differential equations because of the structural change of the network connected to a low impedance load. This system is defined as $\underline{f}_1(\cdot)$. After the fault is cleared, the system structure has again changed and the resulting equations are defined as $\underline{f}_2(\cdot)$.

Figure 2.4.2 shows the resulting state trajectories. The upper left figure is the rotor frequency at each generator. The system electrically splits into two loosely connected islands. The larger frequencies correspond to generators one through three, who support only the light load at bus #10. The lower frequencies correspond to generators four through seven, connected more closely to the heavier load at bus #12. The lower left figure shows the rotor angles. Finally, the right figure is the voltage magnitude at each bus. During the fault, which lasted from time 1 to 1.5 seconds, the voltage is severely depressed. After the fault the voltages recover but then oscillate as the system becomes unstable.

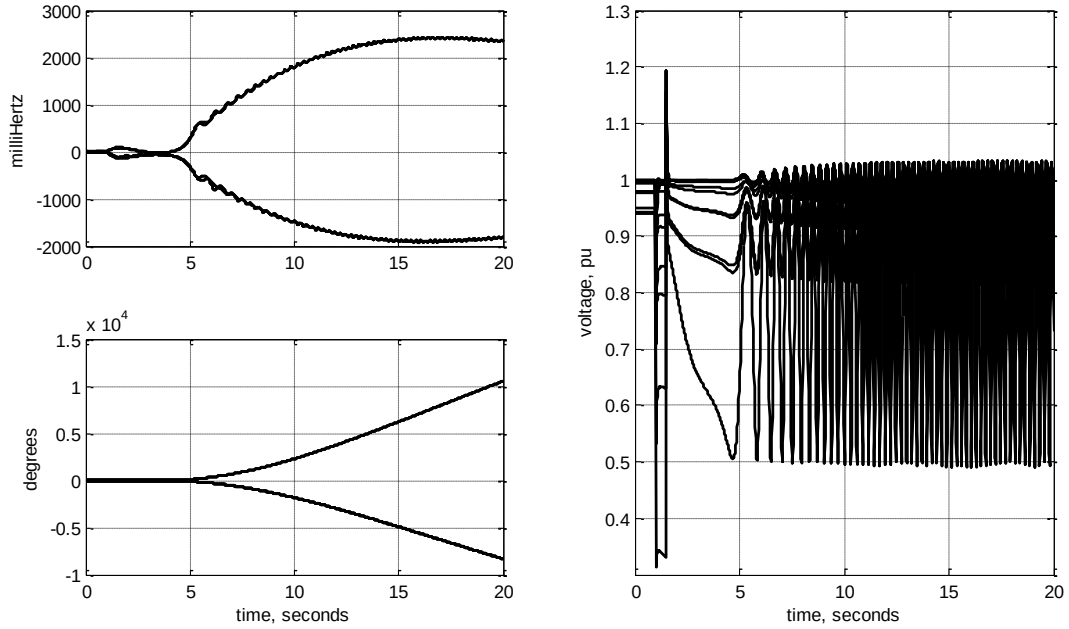

Figure 2.4.2. Long duration fault on line 10-11 prior to clearing.

The minimal solution to recover stability is removing generator #2 and the system becomes defined by $\underline{f}_3(\cdot)$. In this case, because a generator is removed from service, all of its differential equations are also removed. The dimension of the system is reduced by the dimension of the subset defined by the equations of generator #2. Figure 2.4.3 shows the result when this generator is removed at 100 milliseconds after the fault is cleared, followed by removing 16% of the load at bus #12 at 200 milliseconds after the fault is cleared. The system after removing the load is defined as $\underline{f}_4(\cdot)$. So, the dynamical equations for these structural changes are as follows: $\underline{f}_0(\cdot) \rightarrow \underline{f}_1(\cdot) \rightarrow \underline{f}_2(\cdot) \rightarrow \underline{f}_3(\cdot) \rightarrow \underline{f}_4(\cdot)$. The first three sets of vector fields are outside of the actions of the control system. Once guided by the dynamics of $\underline{f}_2(\cdot)$, a hypothetical (as yet, not designed) control system then responds by directing the system to further change through the second two vector fields, and the final system is $\underline{f}_4(\cdot)$.

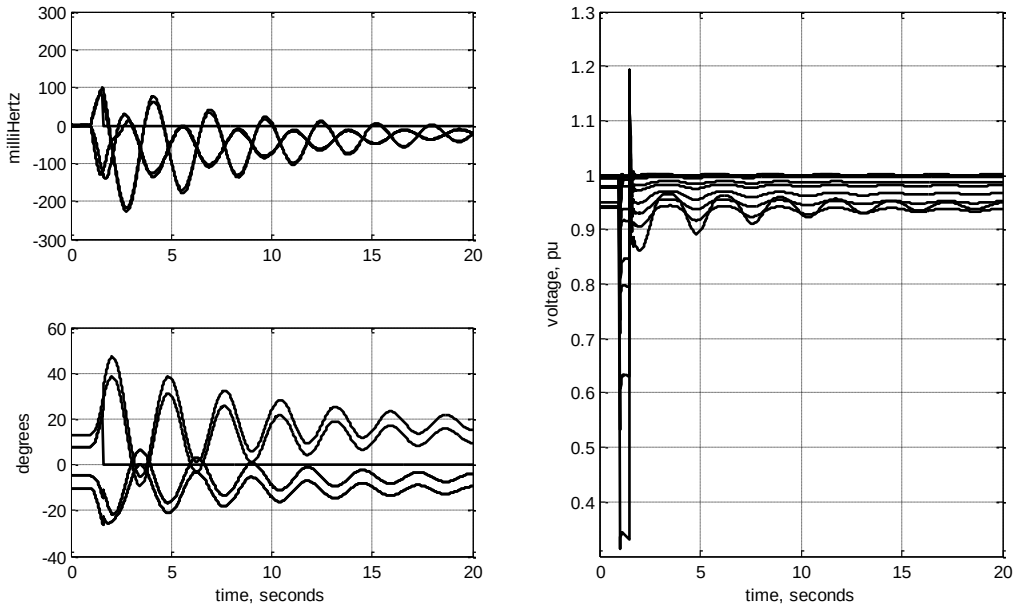

Figure 2.4.3. System response for simple structure sequence.

This control sequence is not the only option available to stabilize the system. In part because of the ability to change the system structure, a large number of control options are available, all with similar final results in the sense that the system is brought to a stable equilibrium point. Control through structural change means the equilibrium point for each option is not the same. Fig. 2.4.4 shows the response when generator #2 is removed at 100 milliseconds after the fault is cleared, $\underline{f_3}(\cdot)$, followed by removing 32% of the load at bus #12 at 200 milliseconds, $\underline{f_5}(\cdot)$, then generator #5 is removed at 300 milliseconds, $\underline{f_6}(\cdot)$. Comparing Fig. 2.4.3 to Fig. 2.4.4 makes it clear that the evolution of the system and the final states are nearly identical for these two different sequences of controls.

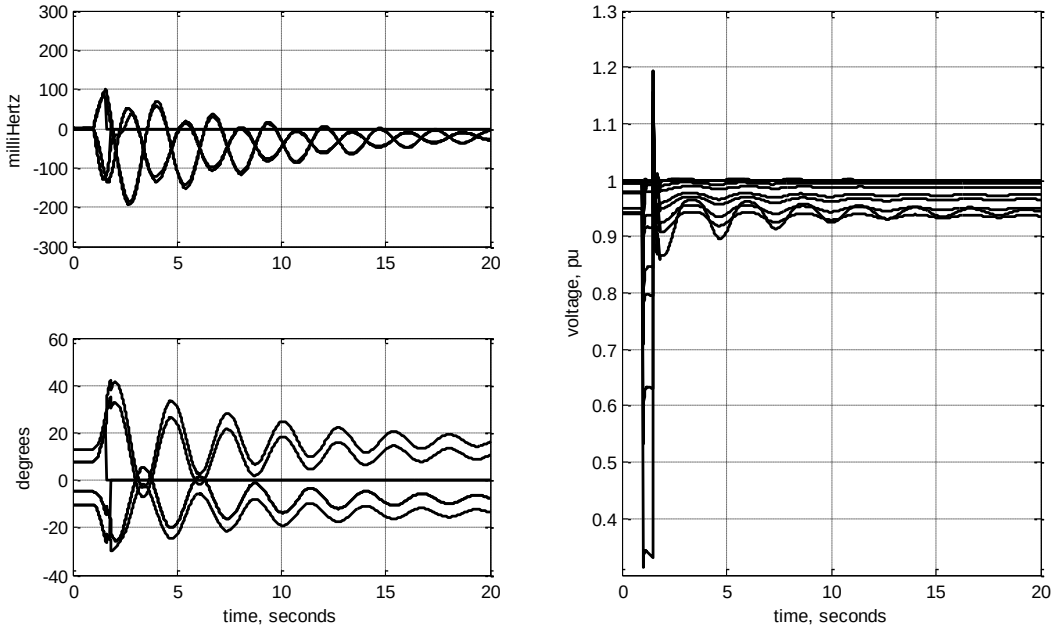

Figure 2.4.4. System response for second structure sequence.

A further example control sequence is tripping generator #2, which is system $\underline{f}_3(\cdot)$, then removing 65% of the load at bus #12, $\underline{f}_7(\cdot)$, then tripping generator #5, now $\underline{f}_8(\cdot)$ because of the load removal, then generator #3, called $\underline{f}_9(\cdot)$, then generator #6, called $\underline{f}_{10}(\cdot)$. The control actions are at 100, 200, 300, 400, and 500 milliseconds after the initial fault is cleared. The result is shown in Fig. 2.4.5. In this case the signals experience a much wider deviation and the final voltage values are low compared to their initial values. However the system response is stabilized.

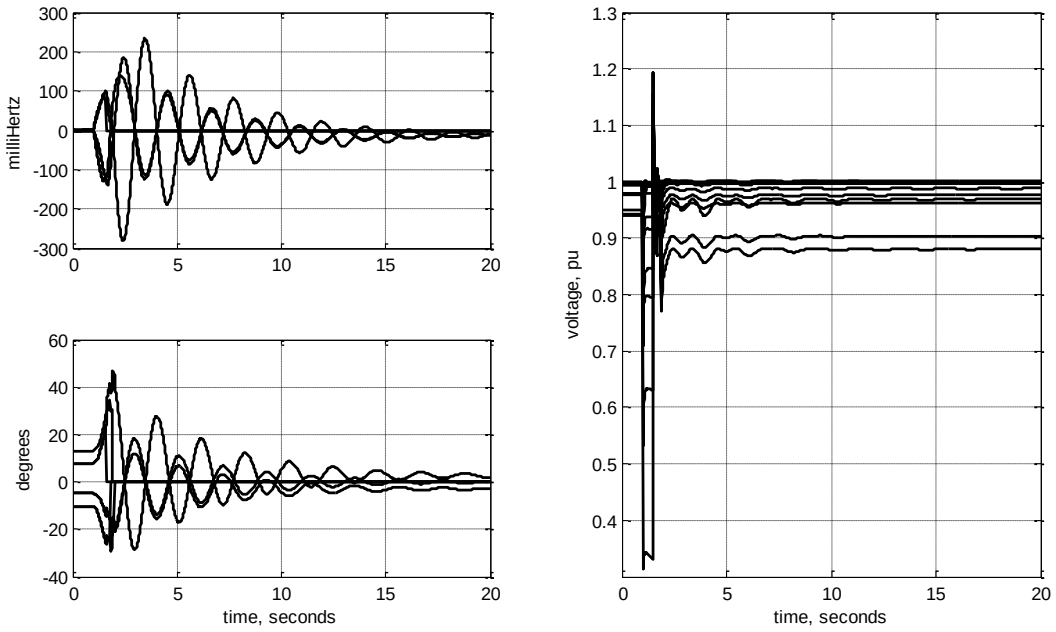

Figure 2.4.5. System response for third structure sequence.

What is needed is a way to quantify the difference between these and other sequence options. This difference then can provide a basis for the design of an algorithmic selection of the best approach. Without such a method, there is no consistent methodology to select between control alternatives. One is left with a system, a disturbance, and a response but no way to know whether that response represents an acceptable cost behavior, or how it compares with other available options. Even when the system is stabilized this result is not necessarily a sufficient outcome because the power system is always eventually stabilized, even during a blackout. A measure of the goodness of the response and the controls selected, compared to other possibilities and compared to a target, is needed.

A solution to this problem is designed here that measures the amount that the evolution of each signal deviates from a desired value. This difference is then numerically integrated over the course of evolution. Prior to summation, each term is squared and the result is a mean squared error. A mean-squared formulation provides a strong signal correlation with good noise immunity [43]. This becomes important later when it is desired to decrease the length over which the measure is computed. The general form of this metric is given in Eqn. 2.4.1. The value Z represents a state of a particular type. The cost of this state, as measured by its deviation from a target Z_j is $C'_Z(j)$. The index i represents a time sequence and the index j represents individual states of type Z. $C'_Z(j)$ is the cost for a specific state j. The cost is computed over a window of size W and is scaled by $\mathcal{Z}$.

$$C'_Z(j) = \frac{1}{W^2}\sum_{i=0}^{W-1}\frac{\left(Z_{j,i} - Z_j\right)^2}{\mathcal{Z}^2} \qquad 2.4.1$$

The total cost for a given type of state is equal to the summation of each individual state value.

$$C_Z = \sum_{j=0}^{M-1} C'_Z(j) \qquad 2.4.2$$

A measure for each of the key signals related to transient stability problems; rotor angle, rotor frequency, and network voltage magnitude; is developed next. Although rotor angle and frequency are fundamental to transient instability, perhaps it is not immediately clear why voltage magnitude is included in the set of state costs. One reason is because control actions may involve removing generation. An advantage of generation tripping is correcting a rotor that has swung past its point of stability. The disadvantage is that a source of reactive power is simultaneously removed from the system. Therefore, a practical reason for including voltage magnitude is to help select controls that compensate for voltage excursions. Also, voltage is a system signal that is required to remain within certain ranges and therefore tracking to select controls that keep it within those ranges is important. Finally, voltage can help anticipate transient instability [21] [30].

For rotor angle there is no time-independent target value available. This is because even in steady state, the angle linearly increases if the frequency is offset from a nominal value. Creating a reference for generating the target value begins by defining a center of inertia angle. Similar to Eqn. 2.4.1, in Eqn. 2.4.3 the index i represents a time sequence and the index j represents individual states. The total number of machines in the system is M. The

inertia of each machine is H. The center of inertia angle represents the angle of a hypothetical machine, rotating at a frequency set by the averaged effect of all machines in the system.

$$\theta_{COI,i} = \frac{\sum_{j=0}^{M-1} H_j \theta_{j,i}}{\sum_{j=0}^{M-1} H_j} \tag{2.4.3}$$

Each machine is then referenced to the center of inertia.

$$\tilde{\theta}_{j,i} = \theta_{j,i} - \theta_{COI,i} \tag{2.4.4}$$

The target value for each machine in the system is set equal to the average of the center of inertia angle, $\bar{\tilde{\theta}}$, over a window of observation. The resulting cost follows from Eqn. 2.4.1 and Eqn. 2.4.4.

$$C'_{\theta}(j) = \frac{1}{W^2} \sum_{i=0}^{W-1} \frac{\left(\tilde{\theta}_{j,i} - \bar{\tilde{\theta}}_j\right)^2}{\pi^2}, \qquad j = 0, \dots, M-1 \tag{2.4.5}$$

The metric for rotor angle is not based on a specific target value of rotor angle. What it is measuring is how much the angle is different from its average, and all referenced to the center of inertia angle. A low cost indicates that the machine angle, referenced to the center of inertia angle, maintains a close proximity to its average value and changes minimally from this value over the measuring window. The metric is normalized so that if the difference is equal to π the cost is unity.

For frequency the cost is based on a reference frequency $\bar{\omega}_j$. This is set to the nominal system frequency in this section, or other values as described later in the dissertation. The normalization is based on the target frequency expected to provide unit cost through ω_{limit}. For example, it is often desired that the frequency of the power system remain within +/- 50 milliHertz of the reference. In this case $\omega_{limit} = 2\pi\left(0.05\ {}^{1}/_{second}\right)$.

$$C'_{\omega}(j) = \frac{1}{W^2}\sum_{i=0}^{W-1}\frac{\left(\omega_{j,i} - \bar{\omega}_j\right)^2}{\omega_{limit}^2}, \qquad j = 0, \dots, M-1 \tag{2.4.6}$$

For voltage magnitude cost is calculated by comparison to a reference voltage $\bar{V}_j$ that is equal to the equilibrium value at each bus prior to a disturbance. Subsequent sections of the dissertation also select other values. The normalization value V_{max} is determined according to the desired voltage limits. A typical value of V_{max} is 0.1 volts.

$$C'_{V}(j) = \frac{1}{W^2}\sum_{i=0}^{W-1}\frac{\left(V_{j,i} - \bar{V}_j\right)^2}{V_{max}^2}, \qquad j = 0, \dots, N-1 \tag{2.4.7}$$

Compute the combined metrics by summation over the individual values.

$$C_{\theta} = \sum_{j=0}^{M-1} C'_{\theta}(j) \tag{2.4.8}$$

$$C_{\omega} = \sum_{j=0}^{M-1} C'_{\omega}(j) \tag{2.4.9}$$

The voltage metric is scaled by $\left({}^{M}/_{N}\right)^{2}$ to account for the difference in number of buses N compared to number of machines M.

$$C_V = \left(\frac{M}{N}\right)^2 \sum_{j=0}^{N-1} C'_V(j) \qquad 2.4.10$$

The total cost of the state deviation is equal to a summation of the individual costs. Applying a summation follows consistently with the approach of summing the individual set of states, Eqn. 2.4.2. It is possible to weight the summation terms, for example giving the rotor angle a higher weight than the voltages for transient stability control. Such further refinements to the general method developed here are not considered but are options in the future to provide possible incremental benefits in control selection.

$$C_{state} = C_\theta + C_\omega + C_V \qquad 2.4.11$$

Now, consider these metric values applied to the various control options considered in the previous example. Table 2.4.1 lists the results. The very large metrics for the case without control actions simply show that the system configuration is unstable. For the second case, the system is stabilized and this is reflected by dramatically smaller cost metrics. The third case results in a slight improvement in the value of all metrics. Finally, the fourth case results in a larger voltage cost metric. For each of these examples, comparison of the metrics with the previous figures shows good correlation between the numerical values and what is expected based on a visual inspection. For example, the third case improves C_ω over the second case, which is consistent with the initial swing of frequency for the second case exceeding -200

milliHertz while the initial swing of frequency for the third case is better than -200 milliHertz. The fourth case voltage cost is significantly higher than that for the second or the third cases and this is reasonable given the generally depressed voltages seen in Fig. 2.4.5.

Table 2.4.1. State cost comparison

Case	Figure #	Control Sequence	C_θ	C_ω	C_V
1	2.4.2	None	1,541,418	165,413	194,327
2	2.4.3	Trip gen #2 @100ms Shed 16% bus #12 @ 200ms	0.0094	0.0236	0.0304
3	2.4.4	Trip gen #2 @ 100ms Shed 32% bus #12 @ 200ms Trip gen #5 @ 300ms	0.0072	0.0162	0.0277
4	2.4.5	Trip gen #2 @ 100ms Shed 65% bus #12 @ 200ms Trip gen #5 @ 300ms Trip gen #3 @ 400ms Trip gen #6 @ 500ms	0.0069	0.0115	0.3454

Based on the results of Table 2.4.1, it might seem that the controls for case #3 are best because they provide the best overall metrics. However, case #3 requires shedding extra loads and tripping an extra generator. Table 2.4.1 does not capture these actions numerically. This

demonstrates that a metric based on the cost of the controls themselves also needs consideration.

One possible solution is to extend the mean-squared error approach to include the control actions. Given u_i as a sequence of control actions leading to a sequence of dynamical systems, Eqn. 2.4.12 shows how the control sequence is referenced against a target control and then normalized.

$$\frac{1}{W^2}\sum_{i=0}^{W-1}\frac{(u_i-u)^2}{U^2} \qquad 2.4.12$$

Summation of Eqn. 2.4.11 with Eqn. 2.4.12 provides the foundation for very common optimal based control methods such as linear quadratic regulators (LQR) [36]. The problem with applying Eqn. 2.4.12 for the class of control problem considered here is the nature of the controls – they are discrete structural changes and single acting. Also, for rotor angle stabilization, the number of controls taken is very small compared to the time-span of the state changes. Another challenge is how to normalize the control costs so that they follow a similar dynamic range as the state variables costs. Although the first case shown previously is an extreme example, it does demonstrate that the state variable costs can vary widely when structures discontinuously change. If control costs are summed with state costs, the dynamic range proves problematic.

A practical consideration when designing a method to measure the cost of the controls is that their values must be set by the effect they have on end-users of the power system, by contractual relationships, or by economics. It is possible to capture these characteristics

mathematically with the mean-square error formulation. But it is a cumbersome approach. For example, the cost relationship between various control options requires backing into the equations to get the desired result. The key reason, however, that makes a solution such as Equation 2.4.12 inappropriate is that, as described previously, controls are not signal based but consist of structural changes. The structural nature of the control does not share the time-series characteristic as the state variables.

The solution to these issues is to not use a mean-squared error metric, Eqn. 2.4.12, for the control costs. Instead, a table relationship for the controls is created. The cost of each control is selected based on the specific characteristics of the system. The following table provides example costs for the kind of controls common in rotor angle stabilization systems.

Table 2.4.2. Set of possible costs for each control.

Structural change control	Example Cost, $\mathcal{C}_j$
System separation	9
Load rejection	8
Generator rejection	7
Dynamic brake	6
Turbine valve control	5
Series Capacitor	4
Shunt capacitor switching	3
Tap-changer control	2
No action	1

The total cost of the controls is then the summation of the individual cost values for the W' structural changes.

$$C_{control} = \sum_{j=0}^{W'-1} C_j \qquad 2.4.13$$

The final metric then consist of the state cost scaled by the control cost.

$$\mathcal{J} = C_{state} C_{control} \qquad 2.4.14$$

The resulting approach to calculating cost has several advantages. It simplifies the process of identifying and quantifying the practical impact of structural changes on end-users of the system. It also avoids the issue of aligning the dynamic range of state trajectory costs and structural change costs. It makes possible combining costs for two fundamentally different aspects of the system – states and structures.

Going back to the example, Table 2.4.3 shows the combined performance metrics, including both state deviation and control costs. Now the minimum cost is for case #2, consistent with the result one might select based on intuition. Table 2.4.3 also is a reminder of a consequence of the metric application method. Metrics are compared to each other when determining which control sequence provides the lowest overall cost. The absolute value of the cost metrics is not important. What matters is how the metrics relate to each other. This is captured by the product form, Eqn. 2.4.14. For example, it is possible to scale all values in Table 2.4.2 by an arbitrary constant factor without impacting the results.

Table 2.4.3. Total cost of each structure sequence.

Case	Figure #	Control Sequence	C_{state}	$C_{control}$	$\mathcal{J}$
1	2.4.2	None	1,901,158	1	1,901,158
2	2.4.3	Trip gen #2 @100ms Shed 16% bus #12 @ 200ms	0.0634	15	0.951
3	2.4.4	Trip gen #2 @ 100ms Shed 32% bus #12 @ 200ms Trip gen #5 @ 300ms	0.0511	22	1.124
4	2.4.5	Trip gen #2 @ 100ms Shed 65% bus #12 @ 200ms Trip gen #5 @ 300ms Trip gen #3 @ 400ms Trip gen #6 @ 500ms	0.3638	36	13.097

Although all of the costs for cases 2, 3, and 4 seem reasonable, the number of controls required for case 4 is significantly higher than for the other cases, and the metric clearly indicates that this selection is suboptimal. At some point the selected sequence of structures becomes so suboptimal that it is unacceptable. When an unacceptable sequence of structures is selected even though a better sequence is available, then the possibility to define the response as control instability arises. By the definitions of this section, the system was stabilized by reducing its dimensionality and all states were brought to their target regions. However, the cost of the controls was unacceptable.

The following is a proposed definition of control instability.

$$\underline{x_K} \in \mathrm{X}, \mathcal{J} > \mathcal{J}_{max}, \mathcal{J}_{available} < \mathcal{J}_{max} \qquad 2.4.15$$

Control instability is when the system is stabilized, but the cost of the controls exceeds a threshold, $\mathcal{J}_{max}$, and there is an available control which achieved the stability objective, Eqn. 2.1.2, with a cost less than $\mathcal{J}_{max}$.

2.5 Summary

This section has provided a framework for systems consisting of structural changes as control. It was shown that control over structure guarantees controllability, as long as removed states are counted in the target domain X. Therefore, a cost-based method of control selection is required. An appropriate cost metric was developed and its utility demonstrated. What is required next is the design of a system to select and implement controls.

3.0 TRANSIENT STABILIY CONTROL WITH MODEL AND PREDICTION

This chapter presents the analysis, design, and validation of a controller acting through structural changes with consideration of the state trajectory and control costs. The design of this section is one realized solution to the ideas developed in Chapter 2. The problem under consideration is large signal rotor angle instability, also known as transient instability.

3.1 Architecture

A controller class that is suitable for nonlinear systems and utilizes a model for iterative prediction is called model predictive control [22]. While all optimal based controllers utilize a model to compute state evolution, what is unique to this approach is application of the model over a finite window, initialized by instantaneous state measurements, and then iterating after each control application. But model prediction is merely a starting point for the work. Like any control system design; whether a methodology for pole placement in a linear feedback controller, an approach to discover a suitable Lyapunov function for stability analysis, or a means to find optimal control solutions for a linear quadratic regulator; a method to apply these ideas is required, along with design and implementation. Application to a system utilizing structural changes as control and oriented towards transient instabilities requires analysis and innovation.

Figure 3.1.1 shows a simplified diagram of operation. Two time regions are illustrated. The first portion, labeled as the evolution region indicates how the state starts at an equilibrium value and then is perturbed by a disturbance at time t_F. The primary class of

disturbances considered here are electrical faults. This condition persists until time t_T. A typical ending condition is removal of the faulted line by existing protection devices in the power system [12].

The controller then applies a model to the starting conditions at time t_T and predicts the future evolution of the system. Knowing the starting conditions requires a time-synchronized set of state measurements. This prediction starts with the case of not applying any controls, and allowing the system to evolve along a path determined by its existing in-place controls, $\underline{f_0}(\cdot)$. Then, the evolution of the system is modeled for each of the stepped structural changes, $\underline{f_1}(\cdot)$, $\underline{f_2}(\cdot)$, …, $\underline{f_K}(\cdot)$, within the set of admissible controls. The performance cost of each future state trajectory is computed with Eqn. 2.4.14 and the best sequence is selected, according to a designed performance metric. Then, the first structure in that sequence is selected and applied to the system. In Fig. 3.1.1 these structures are the control sequences. Utilizing the first structure in the sequence, and ignoring subsequent structures ensures that the controller always acts based on the most recent available information.

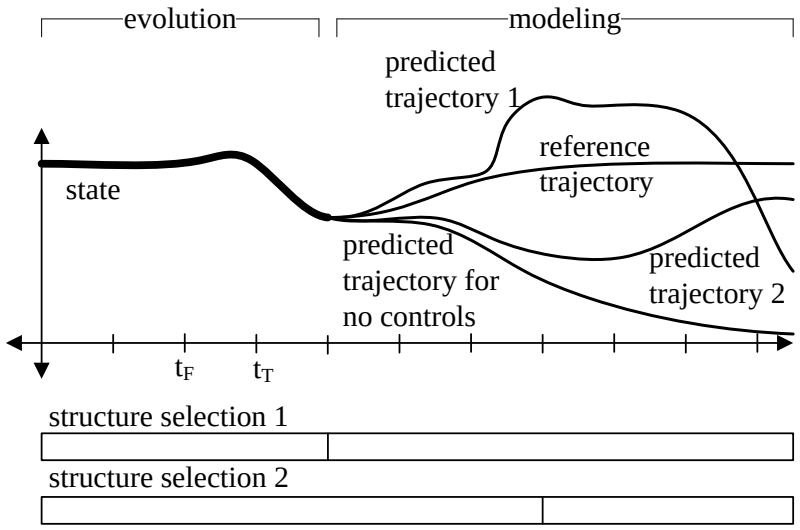

Figure 3.1.1. Evolution and modeling stages of the system and controller.

After the system settles as a result of the structural change, the state is measured again. Similar to the first iteration, individual trajectories are modeled and the best sequence of structures is selected. The first structure from this sequence is applied to the system. This next iteration is shown in Fig. 3.1.2. The controller acts in a feedback manner because after each control application, the state of the system is measured and a new sequence of structures is selected based on the measured state. Controls are applied as a function of state, model, and performance.

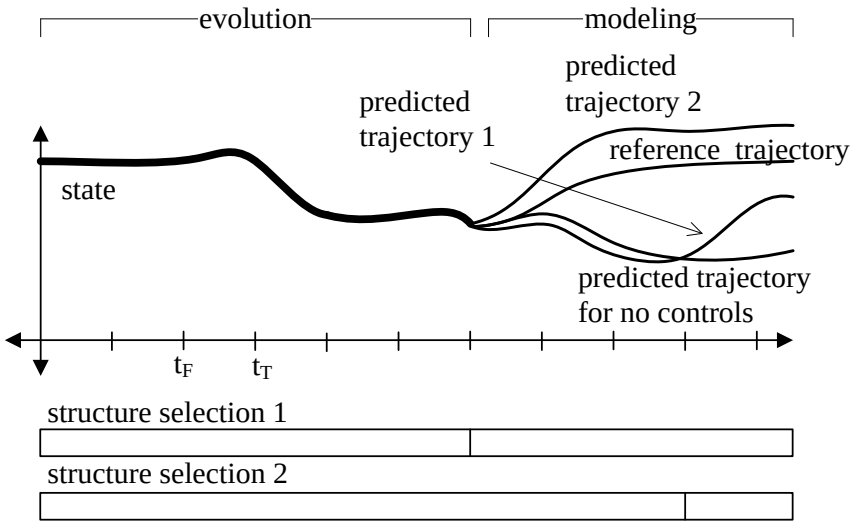

Figure 3.1.2. Evolution and modeling at second iteration.

The previous figures are augmented to include a timeline of the newly designed controller, Fig. 3.1.3, showing when to include control cost calculations. The top timeline in Fig. 3.1.3 shows the events that occur in real-time in the actual system. The lower timeline shows modeled events that occur outside of real-time, during modeled state evolution. An event happens at time t_T and an automatic clearing of that event happens at time t_T. These events are outside of the domain of the controller. The controller is notified of these events either by measuring system conditions or by receiving status information from breakers within the system. In either case, the controller begins operating at time $t_T + t_U$. The time t_U is included to allow time for detection, measurement, and communication delays.

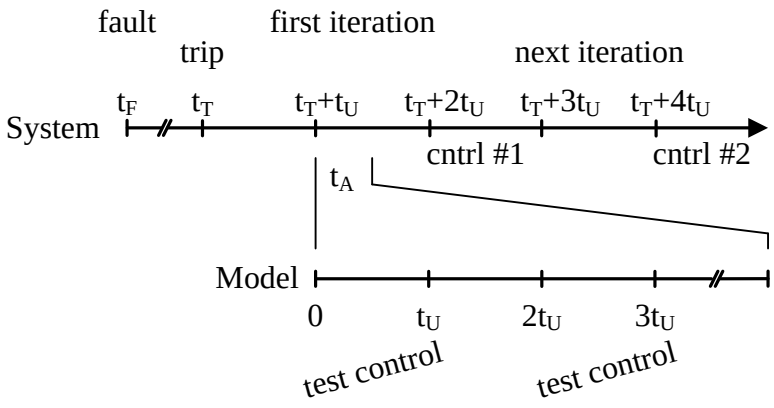

Figure 3.1.3. Control algorithm timeline.

Starting with a measured system state and an estimated model structure and parameters, differential equations enable comparison of the performance of a set of controls within the admissible control set. The time t_A gives allowance for the execution duration. The horizon over which prediction spans depends on the expected dynamics of the system. For transient stability, the important time interval is the first few seconds after t_T. There are two test controls applied as shown in Fig. 3.1.1. The application of a small number of sequential controls is unique to transient stability control. These are not continuous or even discrete-time signal type controls. They are structural changes applied discretely. And, this necessitates a new control approach. One of the structures is tested at time t_U after the algorithm measures the system state and begins modeling. The second is tested at time $3t_U$. The interval t_U between trip time and algorithm initiation allows for system settling and accounts for communication and control mechanical delays. If the algorithm determines no control is necessary, for that iteration, then the next start-time is at $t_T + 2t_U$ instead of $t_T + 3t_U$. After

each algorithm execution a control, if appropriate, is applied to the power system. Then, the system evolves until the next iteration. The state is re-measured and the algorithm iterates again. This process repeats until the system is stabilized.

3.2 The Model

Selection of an appropriate model depends on the class of dynamics and stability under consideration. This work considers large disturbance rotor angle dynamics. These effects are nonlinear in nature and are not linearizable because it is the nonlinearities themselves that can lead to instability. A difficult challenge of electric power system is the stiffness of dynamics, with both very fast and very slow changes that contribute to how the system evolves. For rotor angle, the fast dynamics are the electrical phenomena of the power system transmission lines, transformers, and distribution network. Slower dynamics are the governors controlling thermal and mechanical input power to generators. Also, moderate speed dynamics are in play, such as terminal voltage changes due to an automatic voltage regulator.

One method of dealing with these different time scales is the use of differential algebraic equations (DAE). This approach approximates the network dynamics as being infinitely fast and keeps differential equations only for machine and certain load dynamics.

$$\begin{aligned} \dot{x} &= f_d(x, y, u) \\ 0 &= g_d(x, y, u) \end{aligned} \qquad 3.2.1$$

In Eq. 3.2.1 vector x represents machine and load states while y represents the network states and they are modeled as changing instantaneously. The vector u is a set of in-place controls and d shows explicitly that these equations depend on the system structure. The in-place controls are modeled but not included as part of the controller under design. Each system evolves according to its existing dynamics, including any existing controls. The model developed here is for rotor angle but as long as the disturbance is within the capability of the model and controls selected, finding a control solution is possible for other types of instability.

The machine model selected is 6th order [20]. In the following equations θ is the internal machine angle, ω is the internal machine frequency, and E'_q and E'_d are internal voltages [20]. Model parameters are system inertia H, damping K_D, and time constants T'_{do} and T'_{qo}. The nominal system frequency is ω_s. The power loading of the network is P_g and the current is I_d and I_q. It is assumed that model parameters are known. However, it is unrealistic to assume they are known exactly. During validation of the algorithm random errors are added to the parameters to simulate uncertainty in their values.

The rotor angle depends linearly on rotor frequency. This relationship is captured in the first of the six machine differential equations. The frequency is normalized so its value is unity at nominal frequency, ω_s.

$$\dot{\theta} = (\omega - 1)\omega_s \qquad 3.2.2$$

The frequency rate of change is a function of the difference between machine input power P_m and system load power P_g. When the machine power exceeds the load requirements then the machine accelerates. This is analogous to how a car accelerates when the accelerator pedal is depressed. Similarly, when the machine power is below the load requirements, then the machine decelerates. For the automobile analogy, this is equivalent to the manner in which a car slows down if the accelerator pedal is kept at a constant displacement, while the car begins to climb a hill. The term K_D provides a damping effect which is included to aggregate more complicated aspects of the machine dynamics such as those due to stator winding impedance [20].

$$\dot{\omega} = \frac{1}{2H}\left(P_m - P_g - K_D(\omega - 1)\right) \tag{3.2.3}$$

Two differential equations relate internal flux dynamics. The first is the decay equation associated with the main field axis flux.

$$\dot{E'}_q = \frac{1}{T'_{do}}\left(-E'_q - (X_d - X'_d)I_d + E_{fd}\right) \tag{3.2.4}$$

The second is the decay equation for a rotor amortisseur winding flux, along the quadrature axis.

$$\dot{E'}_d = \frac{1}{T'_{qo}}\left(-E'_d + \left(X_q - X'_q\right)I_q\right) \tag{3.2.5}$$

The model includes an automatic voltage controller, driving the rotor voltage E_{fd}, because it can contribute to rotor angle dynamics.

$$\dot{E_{fd}} = \frac{1}{T_A}\left(-E_{fd} + K_A\left(V_{ref} - V\right)\right) \qquad 3.2.6$$

Governor control is over the generator driving power P_m. In Eqn. 3.2.6 the control time constant is T_A, while the gain is K_A. In Eqn. 3.2.7 the time constant is T_{sg} and the droop is R. The set points are V_{ref} for voltage control and P_c for input power control.

$$\dot{P_m} = \frac{1}{T_{sg}}\left(-P_m + P_c - \frac{1}{R}(\omega - 1)\right) \qquad 3.2.7$$

3.3 State Measurement

Historically, wide-area control of electric power was inhibited by an inability to directly measure the state of the system. This is because of the large geographic area over which power systems are located. When designing a controller for systems such as an airplane, a cell phone, an automobile engine, or even a manufacturing process, the controller and sensors are located together. In contrast, an electric power system may exist over many kilometers. This has made it very difficult to make a system measurement, communicate it to a control location, and have the measurements arrive with values that are closely aligned in time. Until recently, the solution was to measure only the slowly changing values, such as voltage magnitude, estimate values that change rapidly, such as voltage angle, and completely ignore dynamics that change with time scales faster than approximately one second.

The advent of a global positioning system (GPS) helped change this because it provided the ability to put a precise time-stamp on each measurement. Then, it is possible to communicate these measurements across wide distances and when received, time-align them [8]. Missing values are linearly calculated [9][44].

Synchrophasors are measurements of the network states y. In the power system these are complex voltages and currents. Power quantities are also measured. For the model defined according to Eqn. 3.2.2 through 3.2.7 this means good initial values for P_g, I_d, I_q, and V. The technique of time-synchronized measurements is now seeing application for internal machine states as well [15]. Direct time-aligned rotor angle measurements of synchronous machines have been put into service [14]. This means good initial values for θ and ω are available. More recent advancements in measuring the time-stamped state of the power system include detailed machine states such as input power P_m and rotor field signal E_{fd} [16]. It is expected that these technical advancements continue to progress. The work developed here leverages these advances.

The result is that initial values of all state variables in Eqn. 3.2.2 through 3.2.7 are available with the exception of two values: E'_q and E'_d. The challenge with them is that they do not represent physically measureable states. They are an approximation to effects that include state dynamics and neglected damping. So, a method is required to calculate their values based on the other available initial state measurements. First, the terminal voltage and current phasors are measured with time-synchronized accuracy. Then, convert to d-q domain by referencing to the measured machine angle θ. A simple circuit representation of the synchronous machine results in a linear equation for calculating E'_q and E'_d [20].

$$E'_{q-init} = X'_d I_d + V_q$$
$$E'_{d-init} = V_d - X'_q I_q \quad (3.3.1)$$

The results of this section show how all initial values for states are available, either through direct time-synchronized measurements or through a simple calculation. The work of this dissertation is not focused on state observability or estimation. It requires availability of these initial values.

3.4 Performance Metric

At each iteration the applied structural change is selected by determining a control with lowest cost from the admissible set. The cost is calculated following the method of Section 2.4, where each observation window starts with initialized state values.

$$C'_\theta(j,w) = \frac{1}{W^2}\sum_{i=w}^{w+W} \frac{\left(\tilde{\theta}_{j,i} - \bar{\tilde{\theta}}_j\right)^2}{\pi^2} \quad (3.4.1)$$

$$C'_\omega(j,w) = \frac{1}{W^2}\sum_{i=w}^{w+W} \frac{\left(\omega_{j,i} - \omega_{nom}\right)^2}{\omega_{limit}^2} \quad (3.4.2)$$

$$C'_V(j,w) = \frac{1}{W^2}\sum_{i=w}^{w+W} \frac{\left(V_{j,i} - V_{eq,j}\right)^2}{V_{max}^2} \quad (3.4.3)$$

Eqns. 3.4.1, 3.4.2, and 3.4.3 are functions of the state, j, as well as on a start-time index, w. The indices w and i represent intervals of the sample rate f_s. In keeping with the time-scale appropriate for transient stability $f_s = {}^{1}/_{f_{nom}}$. Parameterization of the cost functions by w is necessary to capture the fact that predictions are performed iteratively, each over a separate window. The window start index is w. The window length is W. The value w updates at the start of each prediction iteration, while the parameter W is set during design. To determine state costs, first model the states, with Eqns. 3.2.1 through 3.2.7, over a finite window W sample steps in duration. Then use Eqn. 3.4.1, 3.4.2, and 3.4.3, in Eqn. 2.4.8, 2.4.9, and 2.4.10. The total state cost C_{state} is finally given by Eqn. 2.4.11.

Equations 3.4.1, 3.4.2, and 3.4.3 are different than the related Section 2.4 equations which only depended on j. Previously the performance metric covered a duration that extended until the system reached target region X. However, with a finite window constraint the cost calculation does not necessarily include terminal conditions. This is a limitation when realizing the controller. Performance of the design relies on a good metric along with the iterative nature of structural changes to either bring the system to X or sufficiently close that existing controls bring the system to stability. An advantage of iterating is adaption to changing conditions.

The window length W is selected based on expected system dynamics. It is important that the prediction interval is of sufficient length to capture system evolution as it settles. However, a long window increases the computational demands of the controller. Also, a long window provides additional time for modeling errors to corrupt the prediction. This is

mitigated somewhat by the fact that only the first control action is selected and applied to the system. The most difficult situation is a system described by phenomena with both fast and slow dynamical behavior. A long window is required but that gives additional time for propagation of state initialization error and modeling error in the short-term dynamics. This is in part why the selected model, Eqn. 3.2.1 through Eqn. 3.2.7, includes network through governor aspects. It is a difficult case situation and provides a good test for the algorithm.

The target values in the cost equations are the averaged angle referenced to the center of inertia, $\bar{\bar{\theta}}$, the nominal frequency, ω_{nom}, and the equilibrium voltage values prior to the disturbance, V_{eq}. These values are selected because they are desired operating points and it is expected that as states approach them the system is near the region of convergence of a stable equilibrium point. However, it is important to make clear that these values were not computed based on knowing a stable equilibrium point in advance for the system configuration that exists at time t_T. This is a limitation of control through structural changes. The final topology of the system is not known in advance, nor is its equilibrium point. These target values are near the desired operating conditions of the electric power system and it is a reasonable expectation that these operating points are stable by the design of the system when initially built.

In the model controls are applied for W' individual structure change steps into the future. The value of W' is defined as the control window length. The control cost $C_{control}$ is calculated as the sum of the cost of the individual control actions, Eqn. 2.4.13. The specific values of individual control costs are not fundamentally important to this dissertation. The work is general and allows a wide variety of costs. As an example, a convenient approach is

setting the costs to simple integers, as shown in Table 3.4.1. The values shown here bias the controls against load shedding. This reflects the criticality of electric power to modern society. Specific cost values are system dependent and in a given implementation might differ from the Table 3.4.1 values. The table format is amenable to incorporating specific utility practices or standards. The experimental section demonstrates a variety of control costs.

An important criterion is providing separate costs for when evolution of the system without control application is modeled as either stable or unstable. Differentiation of these cases is by comparing the state cost, Eqn. 2.4.11, with a coarse threshold for the case when no structural changes are directed to the system. When the state cost exceeds a stability threshold then the system without control application is classified as unstable. In this case the cost of acting without control is increased. When the state cost is below the stability threshold then the cost of acting without control is decreased. Table 3.4.1 lists these two cases. The threshold value is derived later.

Table 3.4.1. Control costs selected for experimental verification.

Structural change control action	Base case is modeled stable	Base case is modeled unstable
No control action	1	4
Series capacitance	2	1
Load shedding	4	3
Generator tripping	3	2

The reason to differentiate between these cases is to account for state initialization and model inaccuracy. When the evolution without application of control has a state cost that is within the threshold cost, then it is likely that not executing any controls yields the best result. However, due to modeling inaccuracy or initial state value errors, it is possible that the physical system is not responding this way and is actually moving towards instability. Therefore, the other control actions remain in consideration, although given a higher cost. Alternatively, when the system is moving towards instability, action is needed as soon as possible. However, it is also possible that the physical system is actually responding acceptably. Therefore, the option of not applying any control is kept, but given higher cost.

Optimization is based on minimizing the total cost over all admissible controls. For the reason discussed in Section 2.4, with a nonlinear power system and structural change based control, the approach is total performance metric as a product of state and control costs. Validation of the product objective form is through experimental results.

$$\min_{u_{w,\ldots,w+W'-1}} \{C_{state}(u)C_{control}(u)\} \qquad 3.4.4$$

The selection method is not relevant to the scope of this dissertation. Many well-known approaches are available [34]. However, subsequent chapters provide methods of reducing the admissible control selection space over which Eqn. 3.4.4 applies and introduces methods to decrease the computational burden of this step.

The stability threshold is set based on how the states are expected to perform when the system is moving towards stability. For rotor angle and rotor frequency, this is estimated as

true when the performance metric decays exponentially. Although exponential convergence towards equilibrium is not a dynamic included in the performance metrics, it is a reasonable approximation for stable behavior.

$$\frac{\left(\tilde{\theta}_{j,i} - \bar{\tilde{\theta}}_j\right)^2}{\pi^2} = e^{-\alpha i} \tag{3.4.5}$$

Substitute into Eqn. 3.4.1, and define the resulting measure as the threshold for the rotor angle metric. The window start index is set to zero. Also, the threshold is not a function of the machine state index j.

$$T_\theta = \frac{1}{W^2}\sum_{i=0}^{W-1} e^{-\alpha i} \tag{3.4.6}$$

Apply an equivalence relationship for the sum of an exponential.

$$T_\theta = \frac{1}{W^2}\sum_{i=0}^{W-1} e^{-\alpha i} = \frac{1}{W^2}\frac{1 - e^{-\alpha W}}{1 - e^{-\alpha}} \tag{3.4.7}$$

Similarly for the frequency an exponential decay is expected.

$$\frac{\left(\omega_{j,i} - \omega_{nom}\right)^2}{\omega_{limit}^2} = e^{-\alpha i} \tag{3.4.8}$$

The result is an identical formula to Eqn. 3.4.7 for the frequency threshold.

$$T_{\omega} = \frac{1}{W^2}\frac{1 - e^{-\alpha W}}{1 - e^{-\alpha}} \qquad 3.4.9$$

The exponential constant α is set by forcing the decay to half of its initial value at half of the modeling window length.

$$e^{-\alpha i} = {}^{1}/_{2} \; when \; i = {}^{W}/_{2} \qquad 3.4.10$$

Solving results in the Eqn. 3.4.11 value for α. Alternative approaches to developing a value for α are possible. A larger value of α enforces a faster decay requirement before declaring a system as stable. The control option of not issuing a control in Table 3.4.1 becomes less likely and structural change commands become more likely. Control is biased towards dependability. A smaller value of α means the system can move more slowly to equilibrium and remain considered as becoming stable. This makes it less likely that the controller acts. Control is biased towards security. That is, not acting unless strongly required.

$$\alpha = -{}^{2}/_{W} \, ln({}^{1}/_{2}) \qquad 3.4.11$$

For the voltage metric, exponential decay is not required. The threshold is instead set by estimating that the voltages will stay within $\pm V_{max}$ of the pre-disturbance value V_{eq}.

$$\frac{\left(V_{j,i} - V_{eq,j}\right)^2}{V_{max}^2} = 1 \qquad 3.4.12$$

The voltage threshold then has a simple form.

$$T_V = \frac{1}{W^2}\sum_{i=0}^{W-1} 1 = \frac{1}{W} \tag{3.4.13}$$

The stability threshold is then calculated by substituting Eqn. 3.4.7, Eqn. 3.4.9, and Eqn. 3.4.13 into Eqn. 2.4.11.

$$T_{stab} = \sum_{j=0}^{M-1} T_\theta + \sum_{j=0}^{M-1} T_\omega + \left(\frac{M}{N}\right)^2 \sum_{j=0}^{N-1} T_V \tag{3.4.14}$$

Simplify into a combined expression.

$$T_{stab} = \frac{2M}{W^2}\frac{1-e^{-\alpha W}}{1-e^{-\alpha}} + \frac{M^2}{NW} \tag{3.4.15}$$

As α becomes small T_{stab} becomes large making it more likely the system is estimated as becoming stable, and control actions are less likely. Finally, substitute α from Eqn. 3.4.11.

$$T_{stab} = \frac{3M}{2W^2}\left(\frac{1}{1-\left(\frac{1}{2}\right)^{2/W}}\right) + \frac{M^2}{NW} \tag{3.4.16}$$

This threshold on the state trajectory cost is applied for selecting the cost in Table 3.4.1. All values in Eqn. 3.4.16 are known at the design phase which simplifies implementation.

3.5 Experimental Results

This section investigates performance of the previously derived control approach. First, a specific example is examined in detail. Then, the capability of the controller is investigated through analysis of a large contingency set. As demonstrated in this section transient instability evolves over time-frames of seconds, or even shorter. This means the controller must have a fast response, defined by t_A in Fig. 3.1.3, and is also constrained by t_U in the same figure. The response time is limited by measurement latency (impacting t_U), communication delays (impacting t_U), modeling (impacting t_A through Eqn. 3.2.2 through 3.2.7) and control selection (impacting t_A through Eqn. 3.4.4). The effect of finite computing resources influences selection of the admissible control space, the number of sequential controls W', and the prediction window length W. Later, the admissible control space is restricted to improve computational performance.

This dissertation directed at designing a controller and is not attempting to address implementation approaches. However, given real-time aspirations, the work cannot completely ignore practical implementation constraints and the next two chapters provide designs that significantly reduce computational demands that affect t_A. An interesting tradeoff is between taking longer to make a decision and making a better decision because of more information, compared to making a faster decision and based on less information.

The IEEE 39-bus system, as shown in Fig. 3.5.1, is selected for experimental testing. The contingency set selected is three independent line outages, all simultaneous. The probability of losing three lines in different regions of the system is small. However, this

shows the capability of the proposed approach as it can stabilize such extreme cases. The generation and load power are individually increased by 80% to put the network in a highly stressed state. Loads are modeled as 50% constant impedance and 50% constant power.

The system is setup to remain in the faulted state for 450 milliseconds prior to tripping of the faulted lines. One possible reason for this long time duration is primary protection failing before slower backup protection takes out the lines. This is a further contingency case. The fault condition adds a large amount of energy to the system because the generators spin up, supplying power to large power demands of the low impedance grounding condition. All simulations are with Matlab [45] using custom software to model the system as well as select and apply the controls. A subset of the results was validated with the Powertech Transient Security Assessment Tool [46].

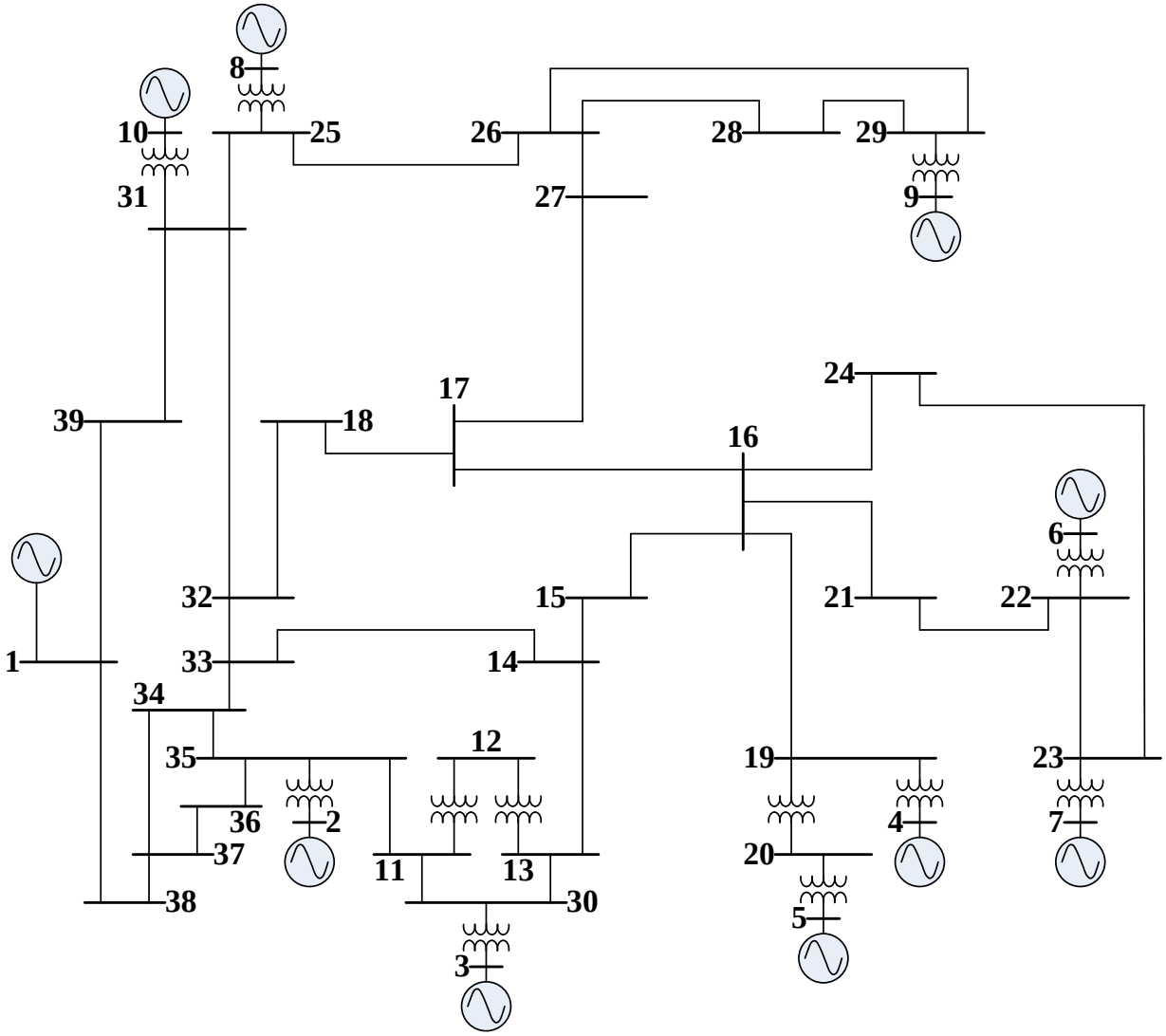

Figure 3.5.1. IEEE 39-bus system.

There are 46 line and transformer connections in the 39-bus system. The result is a total of $\binom{46}{2} = 1{,}035$ double contingency and $\binom{46}{3} = 15{,}180$ triple contingency cases. Triple contingency cases of losing line 17-27 along with all possible double outages are investigated. Line 17-27 is the primary connection to the upper portion of the system. Losing this line results in significant changes to the power-flow. A total of $\binom{45}{2} = 990$ contingencies exist for this set of $N - 3$ cases. From these contingencies, 67 are selected that exhibit transient instability and do not island generators or completely isolate a bus. These are considered here.

Detailed Example

As a specific example, from the set of 67, the case of outages on lines 21-22, 26-28, and 17-27 is considered in detail in this section. This is one of the most difficult contingencies to stabilize from the list of 67. Line 21-22 is very close to generator #6 and during a fault on this line both this generator and generator #7 are accelerated significantly. The lines 26-28 and 17-27 are close to generator #8 and generator #9. This means these generators also experience acceleration during the fault condition. Stabilizing the system, at minimum cost, requires the controller to distinguish between what is happening between these two groups of generators, along with the rest of the system. Furthermore, when line 17-27 is lost, this disconnects the upper section of the power system from its most direct connection to the lower right section (generators #6 and #7).

Simultaneous tripping is selected as a worst case condition. Certainly other sequences of fault and clearing times are possible. Fig. 3.5.2 shows the rotor angles referenced to the

center of inertia (upper left), rotor frequency referenced to the nominal frequency (lower left), and network voltages (right) of the system without any controls applied. Two generators lose synchronization with the rest of the system. These are generators #6 and #7. They are represented by the frequency and angle values that increase to large positive values in the figure. Generator #9 remains synchronized but is in a stressed condition, with low frequency oscillations that are loosely correlated to the rest of the system.

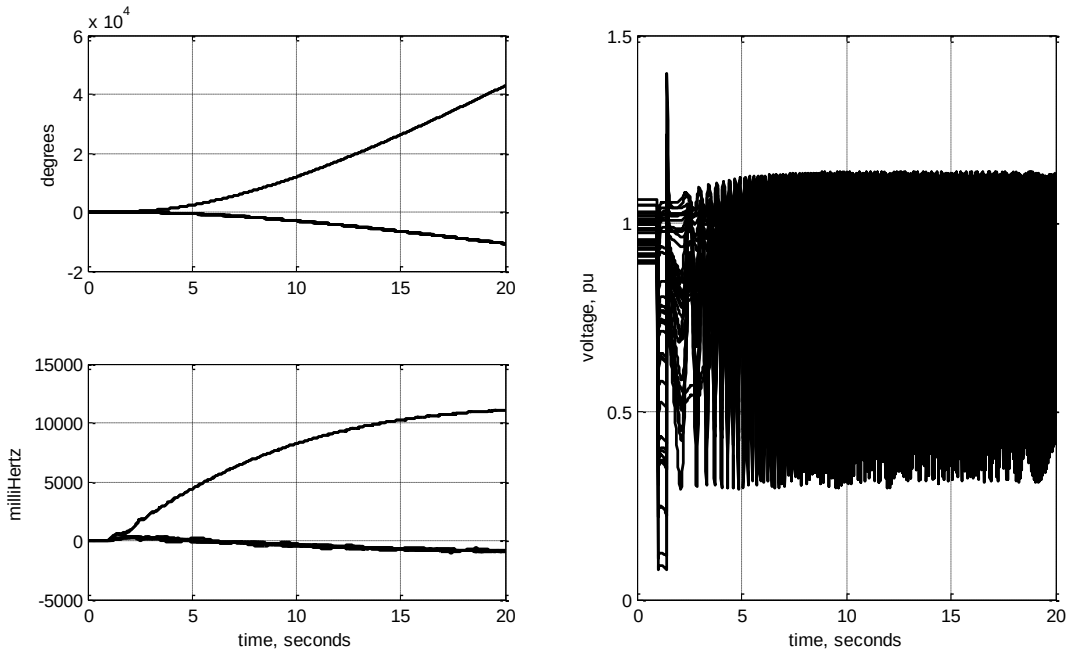

Figure 3.5.2. Response after triple contingency without control.

When the control algorithm executes it first initiates to the present directly measured system state. State is received 50 milliseconds after the line trip is detected. This is at 1.5 seconds in the subsequent tables and figures. This allows 50 milliseconds for implementation

delays, more than adequate given today's communication system capabilities. The set of admissible controls are as follows:

1. Generation tripping: 2, 3, 4, 5, 6, 7, 8, 9, 10.
2. Load shedding in the following sets: {36, 37, 12}, {15, 36, 37}, {16, 20, 15}, {20, 15, 16}, {21, 23, 24}, {23, 24, 21}, {25, 26, 32}, {29, 28, 26}, {32, 25, 26}
3. Series compensation on line 16-17.

A variety of admissible control sets are possible. The next chapter presents a method to select admissible controls dynamically with the intent of reducing the space over which the computationally expensive step of Eqn. 3.4.4 is evaluated, but in a manner that does not significantly lower performance.

Structure changes are selected as acting due to individual controls in the tests. It is also possible to consider pairs of controls, triplets of controls, and further parallel actions. Testing shows that single controls are effective. One advantage of single controls is in acknowledging that the model is not perfectly accurate and therefore taking more significant controls at each iteration can have the negative effect of excess control actions.

The value of W is set for a window length of three seconds. The parameter W' is set for searching over two sequential controls, and t_U is set at 50 milliseconds to account for communication and processing delays. The time sequence diagram of Fig. 3.1.3 is drawn for the case of testing two sequential controls, appropriate for this detailed example with $W' = 2$.

For each sequential set of admissible controls the controller models the trajectory of the system with Eqns. 3.2.1 through 3.2.7. The effect of inaccurate model parameters is included by adding a random 10% error to the parameter values used for modeling. The cost of each control is calculated by the controller with Eqns. 3.4.1, 3.4.2, and 3.4.3. The best structure is selected by finding the lowest cost, per Eqn. 3.4.4. As a result, tripping generator #6 is selected by the controller as the lowest cost option and is applied at 1.55 seconds. Following this, series capacitance is added by the controller to line 16-17 at 1.65 seconds. Finally, at 1.75 seconds, the controller sheds load at bus #25, bus #26, and bus #32. Table 3.5.1 shows the sequence of events for all iterations. Subsequent iterations find further structural changes as having a total cost greater than the cost of applying no controls and the algorithm effectively terminates.

In Table 3.5.1, the systems are identified as $\underline{f_d}(\underline{x})$. The vector $\underline{x}$ represents the complete set of states for a given system structure. The system starts as $\underline{f_0}(\underline{x})$. The fault changes the structure of the system to $\underline{f_1}(\underline{x})$ and then the clearing of the lines further changes the system to $\underline{f_2}(\underline{x})$. Subsequently, the control algorithm is selecting between a set of admissible controls that modify $\underline{f_2}(\underline{x})$ into a new system. This new system has the capability of taking final conditions of $\underline{f_2}(\underline{x})$ as the initial conditions of the new system, then evolving toward a region X under the dynamics of intermediate structure sequences.

Table 3.5.1. Time and description of each event.

Time, seconds	System	Event
0.00	$\underline{f_0}(\underline{x})$	Initial system
1.00	$\underline{f_1}(\underline{x})$	A three phase fault on all three lines occurs simultaneously.
1.45	$\underline{f_2}(\underline{x})$	All lines faults cleared.
1.50	$\underline{f_2}(\underline{x})$	The algorithm begins its first iteration and selects tripping generation #6 as the best first control action.
1.55	$\underline{f_3}(\underline{x})$	The first selected control, tripping generator #6, is taken.
1.60	$\underline{f_3}(\underline{x})$	The algorithm begins its second iteration and selects inserting series compensation on line 16-17 as the best control action.
1.65	$\underline{f_4}(\underline{x})$	The control action is taken.
1.70	$\underline{f_4}(\underline{x})$	The algorithm begins its third iteration and selects load shedding as the best control action.
1.75	$\underline{f_5}(\underline{x})$	Load is shed.
1.85, …	$\underline{f_5}(\underline{x})$	No further controls

Observing the unstable case shown in Fig. 3.5.2 it is evident that removing generator #6, generator #7, or both should stabilize the system. However, when attempted, this solution does not work. What happens is that generator #9 subsequently loses synchronization with the

rest of the system. Application of the optimal control algorithm does trip generator #6 in the set of controls selected in real-time. Then as time progresses and additional sequences of structures are evaluated a set of controls are selected that drive the system towards stability, while simultaneously considering the cost of the state deviations and controls. This is an advantage of the optimality approach towards selecting controls. By monitoring the system in real-time and predicting its response, a solution is found that stabilizes the system with minimal combined control and trajectory cost along the transient evolution towards a stable equilibrium point. The system remains in synchronism by removing the weakest link early, before such generation drags a larger group of generators with it towards an islanded condition.

Fig. 3.5.3 shows the controlled result with the system remaining in synchronism. The large frequency excursion is due to the relatively small size of the system compared to the contingency. If the controller is installed as a full implementation in the field, then other in-place control schemes such as under-frequency load shedding could operate when the frequency reaches such extreme levels. The wide-area control approach described here coordinates well with existing in-place controls. Their effect simply modifies the initial state measurement at each iteration. The controller then determines if the new dynamics require further action, considering both the cost of the controls and the cost of the state trajectory. Alternatively the controller approach developed here is amenable to including in-place control dynamics in the prediction model.

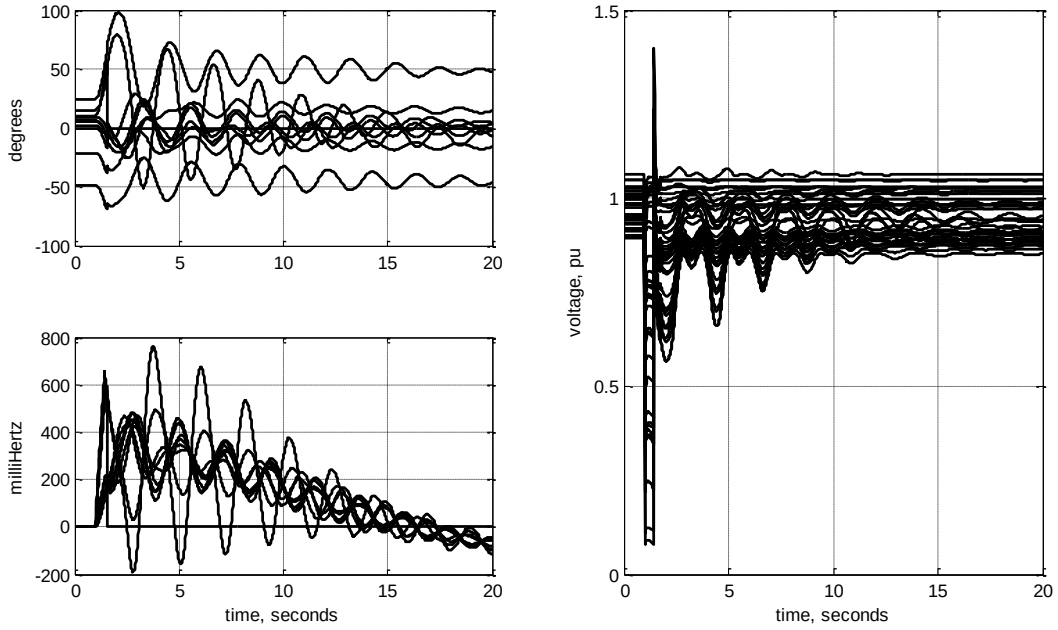

Figure 3.5.3. Response after triple contingency with control.

Comparison Against Exhaustive Search

A test of the algorithm in comparison to an exhaustive search of the best control helps identify the performance loss due to the finite window length and modeling errors. It applies each control action against the exact system, computes the total cost off-line, and selects the control with minimum cost using Eqn. 3.4.4. Testing is performed with a different set of control costs, to investigate the applicability of various cost possibilities.

Table 3.5.2 Control costs for exhaustive search.

Control Action	Base case is modeled stable	Base case is modeled unstable
No control action	1	10
Series capacitance	2	1
Load shedding	10	5
Generator tripping	5	2

Figure 3.5.4 summarizes the results. Comparing the performance of the real-time algorithm against the exhaustive search shows that in most cases the algorithm under non-ideal conditions selects the same controls. Fig. 3.5.4 shows a histogram comparing the number of contingencies out of 67 a given control sequence was selected for both the real-time algorithm (white bars) and exhaustive search (black bars) cases. For all contingencies and for both the exhaustive search and real-time algorithm the system is stabilized.

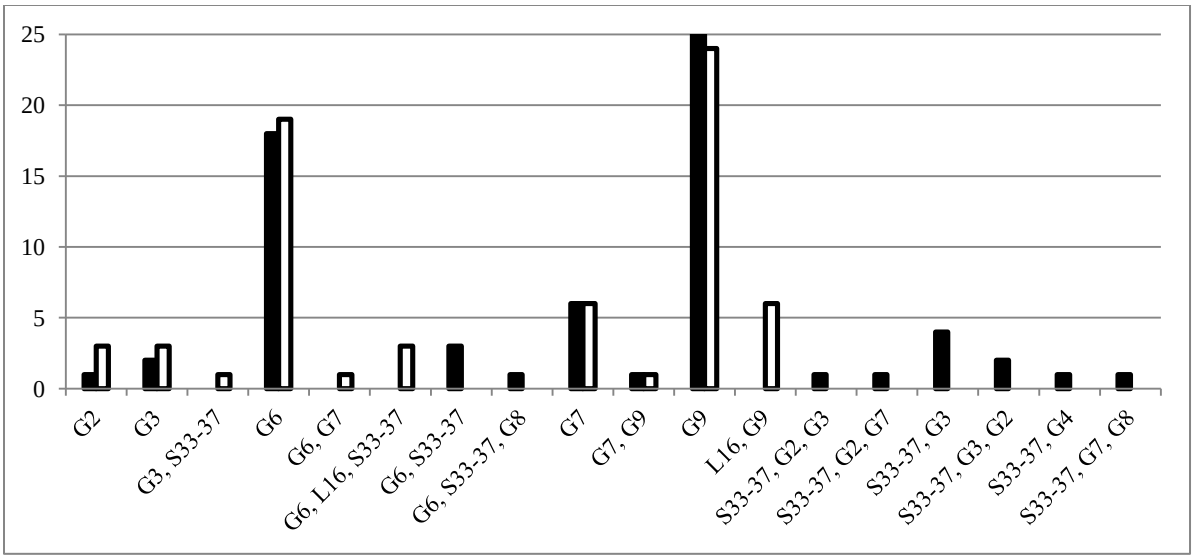

Figure 3.5.4. Histogram of control actions.

As an example of the performance tradeoff due to non-ideal conditions, here is one case where the real-time algorithm selected a different control sequence: losing lines 13-14, 34-35, and 17-27. The exhaustive search first shed load, then followed by tripping generator #3, and then tripping generator #2. The real-time algorithm selected tripping generator #3 first and shedding load.

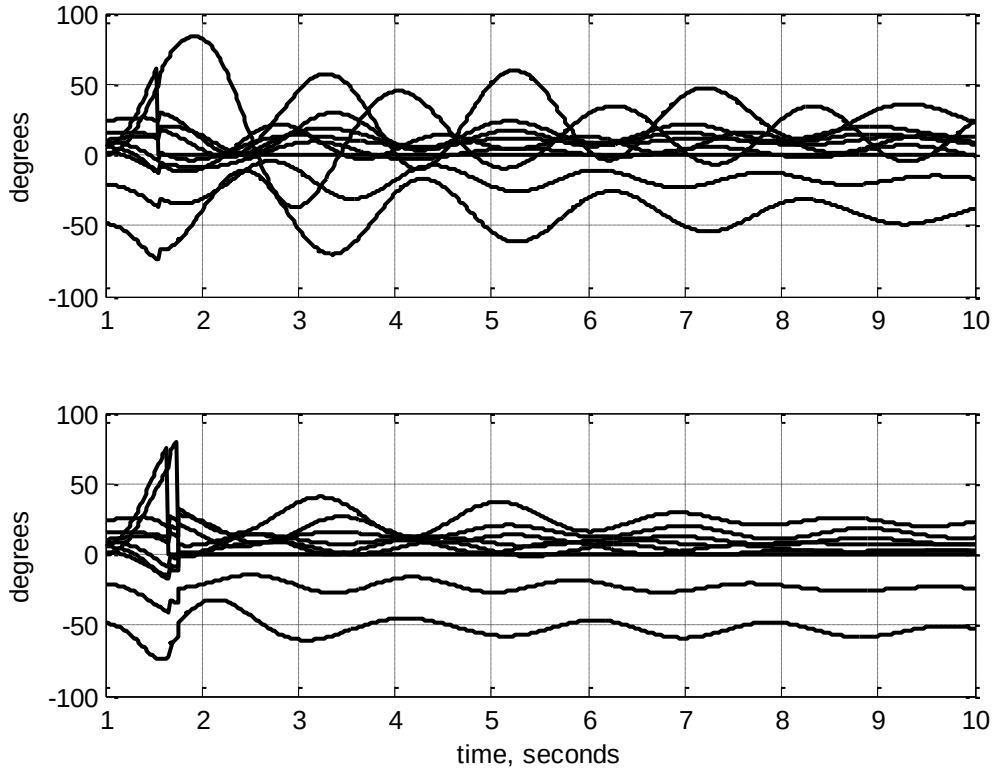

Figure 3.5.5. Comparison of control selection methods.

Fig. 3.5.5 shows the rotor angles for the sequence of controls selected by the real-time algorithm (upper figure) and the sequence of controls selected by the off-line search (lower figure). The rotor angles swing over a wider range for the real-time control case, but the system is stabilized. Reducing some of the limitations on the real-time algorithm, for example allowing for a longer modeling window or a larger number of sequential controls results in the real-time algorithm achieving the same performance as the exhaustive search.

Performance During Unexpected Contingencies

The iterative and feedback nature of the algorithm developed here provides robustness against unexpected conditions. One problem that can occur in electric power systems is an actuation failure. For example, if a breaker is ordered to open a line, shed load, or trip a generator, it can sometimes fail to operate. This case is somewhat unique to the control of electric power systems, compared to other types of control. For a more traditional signal style control input the continuous or stepped nature of the controller can make the onset and consequence of the failure less unexpected. In a power system, the breaker might only have to respond once every few years. Until the time it attempts to operate, if there is no advanced information regarding its suitability, then it could fail without warning.

Therefore, when control is over the structure of a system such as electric power, the ability to recover from this type of failure is important. In fact, it is appropriate to consider this type of failure as an additional contingency case. To test these conditions, a set of experiments is run for the non-ideal conditions where the first attempt at an action fails. These experiments are for all 67 of the three-line outage contingencies. After detecting that the attempted change was unsuccessful for capacitance switching or load shedding, the selected control is removed from consideration by the algorithm because of the possibility that the failure is permanent. There is little point in wasting additional time trying the control again. For generator tripping, a backup scheme removes the generator after an additional 100 millisecond delay. The control algorithm remains able to stabilize the system. This shows the advantage of the feedback mechanism that is measuring the state and dynamically adapting the controls to the evolving system conditions.

Returning to the detailed example, a test is setup with the first generation trip action initially failing and then delayed by 100 milliseconds before removal by a backup system. The result is tripping of generator #6 at time 1.65 seconds. This is in contrast to when the same generator was removed in the initial example without an actuation failure. As shown in Table 3.5.1, generator #6 was removed by the control system at 1.55 seconds in the initial example. Subsequently, at 1.75 seconds, the controller with actuation failure sheds the same loads (bus #25, #26, and #32) as was selected for shedding in the example without control failure. However, capacitor insertion is not taken as an action.

In the previous example, when the control was not delayed, the system stabilized after the load shedding structural change control action. However, with the actuation failure, the system remains unstable. The controller in the present example senses this instability and removes generator #7 at 1.85 seconds. The system response after this control action leads to a seemingly stable state, but only temporarily. During this time of temporary stability, generator #9 experiences an oscillation that slowly grows. For approximately eight seconds the system remains in a tenuous state. Finally, generator #9 goes out-of-step with the rest of the system.

The advantage of the feedback controller is its ability to respond to the evolving instability. Before the system becomes completely unstable, at 6.983 seconds, the controller sheds more load. The system stabilizes by keeping all generators closer to the swing of generator #9. Figure 3.5.6 shows the response of the system when this last control is artificially blocked. It is generator #9 that accelerates away from the rest of the system with an increasing frequency. Figure 3.5.7 shows the complete response, with all of the actions selected by the controller applied correctly.

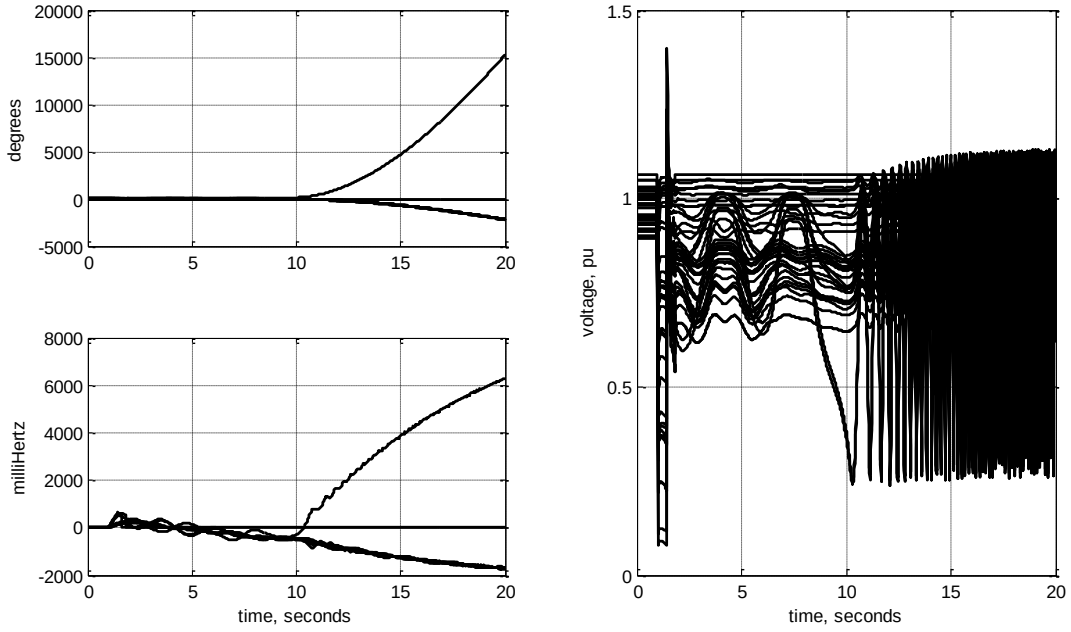

Figure 3.5.6. Response of the system with last control artificially blocked.

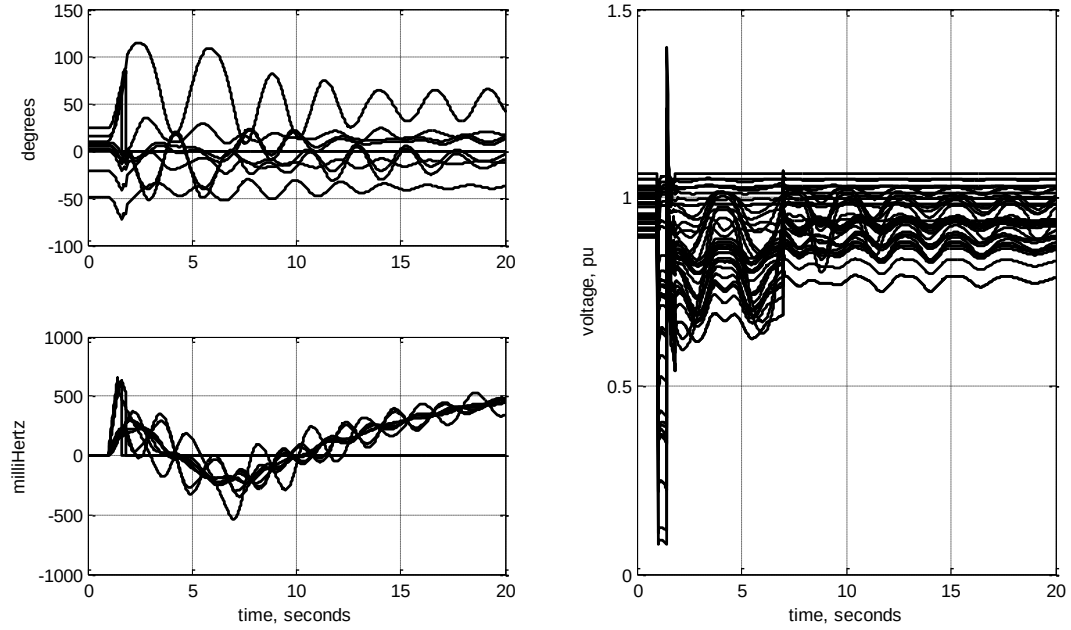

Figure 3.5.7. Response with all selected controls applied.

Control Instability

It was shown previously that when changing the system structure is an available control option, as it is in electric power systems, there is a possibility for control actions to stabilize the system but at an unacceptable cost. To investigate this condition, the cost allocation in Table 3.4.1 is set equal for all controls, and the no-control case set to twice the cost of the others. This biases the system towards selecting a control action over not selecting a control action.

This set of costs is compared against the original set of costs for the contingency of losing lines 17-27, 16-21, and 17-18. The result of this outage is separation of most direct connection between the lower right side of the power system and the rest of the power system. Without controls the generators at terminals #4, #5, #6, and #7 lose synchronization with the rest of the system. The real-time control algorithm selects tripping generator #7 as the lowest cost option and this is applied 50 milliseconds after the fault is cleared. The system then stabilizes.

The result with the new set of costs is removing generator #7 at 1.55 seconds, shedding load at time 1.65 seconds, removing generator #2 at 1.75 seconds, and removing generator #10 at 1.85 seconds. While the system is stabilized, the case with modified control costs does so with a much larger number of required control actions. One might consider this type of operation as a form of control instability. Although the system is stabilized, the controls act excessively.

4.0 THE CLASSIFICATION CONTROL METHOD

In the previous chapter a controller which applies optimality principles for selecting a sequence of structures to bring transiently unstable power systems to an acceptable operating point is designed, analyzed, and validated. The approach is shown to effectively control even large contingency events. However, a disadvantage of the method is requiring a significant number of calculations. Computational performance is particularly relevant for large disturbance rotor-angle control. This type of instability acts over short time intervals and therefore response time of the controller is critical. The minimum achievable response time is a function of the time it takes to select each new control action and techniques to reduce this selection time are needed. Helping offset these tradeoffs are advances in computing power and installation of higher performance computer networks [17].

When optimal control is applied to linear systems with feedback, the Riccati equation solution is available, providing a reasonably fast control selection [36]. For nonlinear systems, linearization is sometimes possible, which then allows Riccati based control for selecting the feedback gain. Linearization is not an option for large signal transient control because it is precisely the nonlinear nature of rotor angles dynamics that drive the instability. These nonlinear phenomena are important for the controller to capture.

An approach to decreasing the computational demands of nonlinear system optimization is numerical quantization of states and then using linear programming for control selection [34]. Of course, brute-force search is always an option. The performance of both these approaches is improved by reducing the space of available controls. This chapter

constructs a method to reduce the set of admissible controls, meaning admissible sequences of structures, based on an algorithm that adapts the search space as the controls execute. The reduction is constructed to keep controls most likely to contribute towards a solution with acceptable cost.

4.1 Admissible Control Subspace Classification

Fig. 4.1.1 shows subsets of the control space. This section describes how classifying the control space leads to an approach for considering fewer controls during optimization. The set A in Fig. 4.1.1 includes all admissible controls and it is this set over which an optimal control searches, in existing approaches [35]. Admissibility means the controls meet constraints over an entire interval of application. For example, in an electric power system a shunt capacitor at a certain location might improve performance but is not physically installed. Therefore it is not available for switching into service and is not an admissible control. Other constraints include contractual obligations on load changes, device cycling interval limitations, or constraints on actuation ranges.

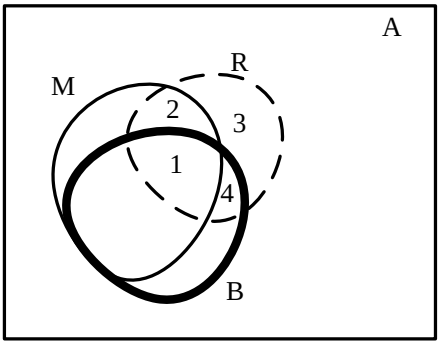

Figure 4.1.1. Admissible control subspaces.

The thick-lined region, B, is the subset of available controls which achieve a cost less than an acceptable cost. An acceptable cost means that the system is stabilized, states remain as close as required to acceptable ranges, and the cost of the controls is satisfactory. As demonstrated earlier, multiple structure sequences are usually available that stabilize the system with acceptable cost. Of course, as the acceptable cost becomes smaller, so does region B. Region B includes the globally optimal control sequence for a given set of admissible controls, and a given definition of cost.

The region M is the subset of controls modeled by the implemented controller to achieve a cost less than an acceptable cost. Suboptimal conditions result in $M \cap B \neq B$. A factor contributing to these suboptimal conditions includes inaccuracies in the model used for control selection. Parameters of the model can have errors and in some cases the structure of the model itself is incorrect. Also, the measured starting state for the model includes sensor noise. This results in the model not making an accurate assessment of the following system dynamics. Another condition leading to errors is the length of the window over which the model acts. In the ideal case the model is applied over a window of sufficient length to bring the system to its desired final state, or at least of sufficient length to capture most of the system settling time. In reality, computational constraints necessitates a finite window length. Also, because of model inaccuracy, there is benefit in iterating its application and applying a finite window for control selection. Then, at each iteration, a new starting state is measured and a new set of controls are selected. This is the method considered here.

The dashed region R is a subset of restricted controls, selected to reduce the search space over which the model is applied. The intent is to apply the control algorithm only over

the controls of subspace R instead of over the entire space of admissible controls A. The objective of this work is defining region R. Furthermore, an objective of this work is to define region R with a computational cost less than simply applying each control sequence to the model, as was done in the previous chapter. As demonstrated in Fig. 4.1.1, four subspaces are relevant.

Table 4.1.1. Admissible control subspace descriptions.

$R1$	These controls achieve an acceptable cost both under modeled conditions and when applied to the physical system.
$R2$	These controls are modeled to achieve an acceptable cost but when applied to the actual power system the resulting cost is larger than acceptable.
$R3$	These controls do not achieve an acceptable level of cost.
$R4$	These controls are not modeled to achieve a desired cost but if applied to the physical system the resulting cost is acceptable.

The goal is subset R as small as possible. This minimizes the controller search space and therefore improves overall search performance. In the ideal case $R1 = R$ while $R2 = R3 = R4 = \emptyset$. The subset $R2$ is a problem because it could lead to a selected control which then performs poorly when applied to the physical system. The subsets $R3$ and $R4$ are a problem because they unnecessarily increase the computational demands, while not contributing towards the eventual solution. Computational demands impact time t_A in Fig. 3.1.3 and therefore increases the response time of the controller. Although none of the

controls in subsets $R3$ or $R4$ are selected, they force the controller to take longer before making a control decision. This has a destabilizing effect on the performance of the system state trajectories. The states swing over wider ranges and more complicated and wide ranging structural changes are required for stabilization. Therefore, it is desired to keep subsets $R3$ and $R4$ as small as possible.

The numerical size of spaces A and R in Fig. 4.1.1 is determined by the number of controls considered and the number of sequential intervals over which those controls are applied. Let N_A be the total number of available controls, implemented as structural changes, contributing to set A. For example, if control options are removing generation at each of five buses and adding electrical braking loads at each of four buses then $N_A = 5 + 4 = 9$. From these controls, actions are applied as sequences. A given sequence for the previous example might be adding a braking load at a given bus and then removing a generator at another bus. So, two of the controls are applied in sequence. Let $\mathcal{N}_A$ be the number of sequences of structural changes available as a result of the individual structural change control actions included in A. It is the value of $\mathcal{N}_A$ with direct impact on computational performance. The control selection algorithm selects sequences of actions from A, applies each to a model that is initialized with real-time power system measurements, and selects the sequence of controls which minimize a cost objective.

Let W' be the number of sequential controls considered, with $W' < N_A$. In most cases, $W' \ll N_A$. After a sequence of control is selected, the first one is applied to the electric power system. Then, the selection algorithm repeats with a new set of initial state measurements. The previous chapter demonstrated that a value of $W' = 2$ was sufficient to stabilize even

large contingencies. This is due to the nature of rotor angle instability. A relatively few number of structural changes are sufficient to bring the system into order. This helps keep the computational demands low.

For the initial control selection, the search space over which optimization Eqn. 3.4.4 selects is $N_A + 1$ in series over a window of W'. The unit addition accounts for the fact that not issuing any controls is kept as a valid option. Then, at each subsequent sequential consideration, one less control is available because repeated controls are not allowed (see constraint #3 of Section 2.1). A calculation of the total number of controls considered at each iteration starts with Eqn. 4.1.1.

$$\mathcal{N}_A = \prod_{k=0}^{W'-1} N_A + 1 - k \qquad 4.1.1$$

Before tackling more sophisticated approaches to reduce the computational demands of Eqn. 4.1.1, an easy first step is to not allow control sequences that start without a control action. There is little gained by waiting before applying controls. Eliminating these cases as options reduces $\mathcal{N}_A$. However, repeating the no control action is allowed as it is sometimes advantageous to wait between control actions. Fig. 4.1.2 summarizes the number of sequences $\mathcal{N}_A$ as a function of the number of individual controls N_A, since the relationship is slightly more complicated than Eqn. 4.1.1 alone. The upper figure is for $W' = 2$ and the lower figure is for $W' = 3$. The nonlinear relationship between the number of controls N_A and the number of sequences that the controller must consider helps demonstrate the advantage of finding a subset R in A with N_R smaller than N_A. Even a slight improvement in N_A leads to dramatic

improvements in the number of controls considered using R as the admissible control space instead of A as the admissible control space.

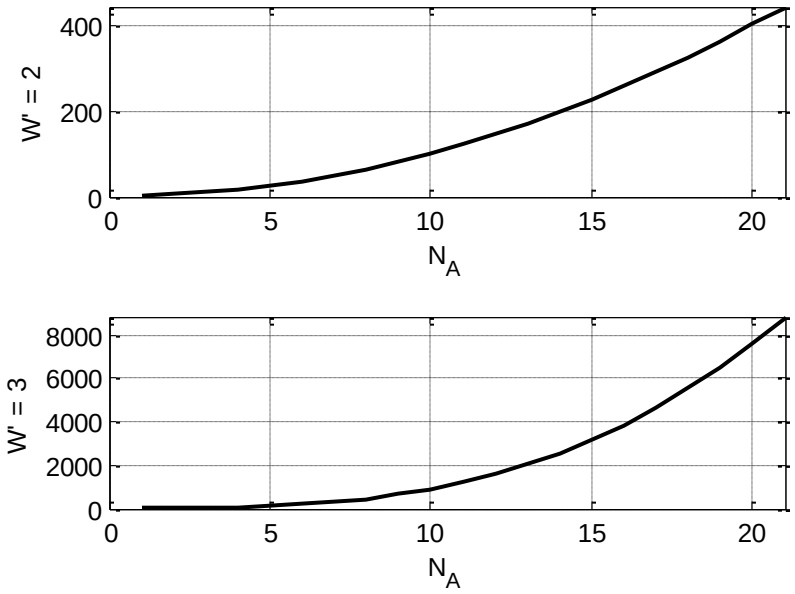

Figure 4.1.2. Number of control sequences $\mathcal{N}_A$.

4.2 Subset Classification Algorithm

This section describes the classification algorithm for selection of controls in subset R, with the intent of $R1$ as large as possible. It is based on measuring the system state immediately after a disturbance. Then, the state of the system with no controls applied is projected, according to a model, for a finite horizon into the future. From this single prediction, a subset of controls is selected for consideration by the optimization algorithm. Determining this set of controls adaptively, based on the measured system state, results in a

smaller set of controls to consider than if the controls are selected prior to the start of the disturbance.

Three types of states are monitored when selecting the appropriate control. These are the rotor angle θ, rotor frequency ω, and bus voltage magnitude V. The costs are calculated as the deviation from targets, according to Eqn. 3.4.1, 3.4.2, and 3.4.3 for predictions without controls applied. The resulting values are $C'_{\theta}(j,w)$, $C'_{\omega}(j,w)$, and $C'_{V}(j,w)$, where j represents a given state and w is the starting index of the window. There is a different cost value for each state and for each window starting time index. States range over either M generators or over N network buses.

Reduction of the search space is based on identifying relationships as independent as possible between control actions and the cost related to an associated single type of state. For three cost equations, the proposed approach selects three types of controls and relates each to a dominant effect on these states. The controls considered in this chapter are generator tripping, load shedding, and shunt capacitance adjustment.

The clearest relationship between a control action and a single state type is the way generator tripping directly effects an unstable rotor angle state. Therefore, the generator tripping control is associated with $C'_{\theta}(j,w)$. The load shedding control is associated with $C'_{\omega}(j,w)$ because of the well-known relationship between frequency ω and the machine T_m compared to load T_e torque.

$$J\frac{d\omega}{dt} \propto T_m - T_e \qquad 4.2.1$$

Shedding load directly impacts ω through T_e, and then cost through Eqn. 3.4.2. Finally, shunt capacitance insertion is associated with $C'_V(j,w)$ as reactive power injection and voltage level are related [47].

Selection of a reduced set of controls proceeds as follows for generation tripping. First, rank the costs $C'_\theta(j,w)$ in order from largest to smallest. Include only those generators in the set $j \in \{1,\dots,M\}$ which have not previously been removed by a control action. Define this list of generators as $\Gamma_{rank,\theta}$. In this list, the machine with the highest cost $C'_\theta(j,w)$ is denoted as $j = J$. Next, determine the frequency at the terminal modeling window index $w + W$ for machine J. This frequency is defined as $\omega_{J,W}$. This frequency becomes the basis for collecting generators into two sets; those with frequency at the terminal window time near $\omega_{J,W}$ and those not near this frequency. The distinguishing criterion between these two sets is based on the maximum frequency difference, scaled by free parameter ζ.

$$\Delta\omega_{crit} \equiv \zeta \, max\left|\omega_{j,W} - \omega_{J,W}\right| \qquad 4.2.2$$

The maximum is computed over all $j \in \Gamma_{rank,\theta}$. For this work the parameter is set as $\zeta = {}^1/_2$. The subset Γ_θ of generators available to consider for removal as a control action are those in set $\Gamma_{rank,\theta}$ starting with the machine associated with the highest cost, and continuing until a machine is found with frequency $\left|\omega_{j,W} - \omega_{J,W}\right| > \Delta\omega_{crit}$. This algorithm gives two benefits. First, it ensures related frequency swing directionality for generators in set R. Second, the

collection of generators in R stops once a generator is found with sufficient frequency difference from the machine J. This minimizes the number of considered generators.

As a numerical example, consider the case where $M = 4$ and the cost $C'_\theta(j,w)$ for each rotor angle state are given by $C'_\theta(j,w) = \{2, 0.5, 0.1, 1.5\}$ where the array is indexing by machine j. Assume also that the frequency of each state at the terminal window time is $\omega_{j,W} = \{2, 0.5, 0.1, 1.5\}$. For simplicity of illustration these two sets use the same numerical values. From the set of $C'_\theta(j,w)$ values it is clear that $J = 1$, $\Gamma_{rank,\theta} = \{1,4,2,3\}$ and from Eqn. 4.2.2 the frequency criteria is $\Delta\omega_{crit} = \frac{1}{2}|0.1 - 2| = 0.95$. Therefore, the generators selected as available for tripping commands are #1 and #4 because they have the highest cost and also with frequency difference less than the criteria frequency. This is the reduced set of controls Γ_θ subsequently input to the optimization search algorithm. For this example $\Gamma_\theta = \{1,4\}$.

Motivation for this selection method is because during transient instability, generators often separate into relatively coherent subgroups [27]. Fig. 4.2.1 shows an example of transient instability for the IEEE 39-bus system. Four of the ten generators accelerate away from the remaining six generators. The horizontal dashed line is a separation point based on the criteria frequency $\Delta\omega_{crit}$. Because Fig. 4.2.1 shows a clear separation it might seem that only the terminal frequency is necessary, without also ranking based on cost Eqn. 4.2.1. However, in many cases the separation is not as distinct and the advantage of applying ranked costs is a quantitative measure of which generator states are most different from the target values and therefore result in the highest benefit from controlling. Although not the preferred

result, the classification algorithm is robust to the case when the system separates into less or more groups. In such rare cases, when the selected set of controls is larger than necessary it impacts computational performance.

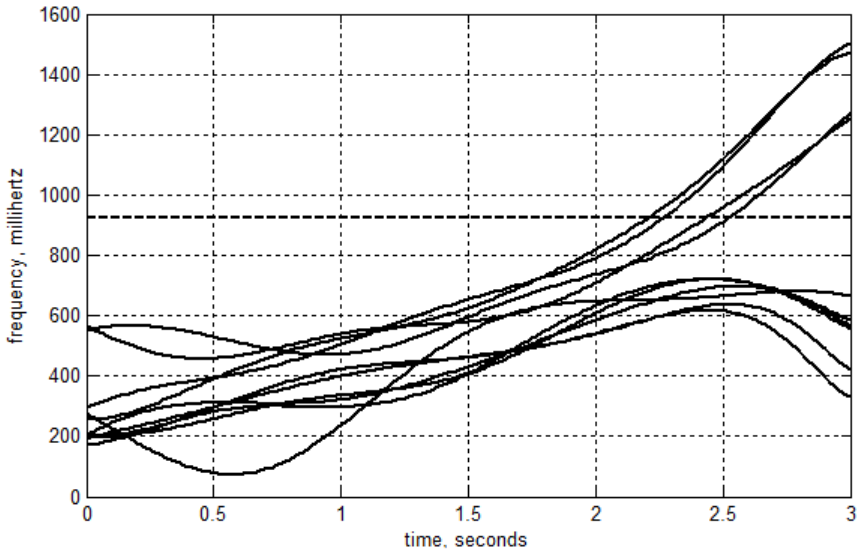

Figure 4.2.1. Frequency separation example.

Load shedding is based on arranging costs $C'_{\omega}(j,w)$, ordering each from highest to lowest. There are M generators and N buses, typically with $N \gg M$. Each bus may or may not include an available load for shedding. Therefore, the first load encountered while traversing the network away from a given generator is selected for consideration in the load shedding control scheme. Because of the important nature of power system loads it is expected that their selection is unique to each implementation. The controller cannot shed critical loads and

other loads might have contractual availability for shedding. The algorithm is easily extensible for constraints specific to each power system implementation.

It is possible for the classification approach to select loads in R for regions where the frequency is moving away in the positive direction. In this case it might seem unlikely that the load will be further selected for shedding by the subsequent control algorithm. However, the predictive scheme is considering sets of controls that includes generation removal and such actions can result in frequency subsequently moving the opposite direction. Therefore, it is preferred when selecting set R to keep the highest cost loads, according to Eqn. 3.4.2, independent of the local frequency.

For shunt capacitance insertion, after computing the costs $C'_V(j,w)$ a single bus with the highest cost and with a connected shunt device is selected for inclusion in the optimization search. If during the control sequence a shunt capacitor is switched into service, then further control with capacitance is disabled. This avoids potential issues with excessive selection of this control option with short windows for prediction. The control cost of inserting a shunt capacitor is much less than the control cost of tripping a generator or shedding load. Therefore, it is possible that the algorithm could inappropriately continue to select this control option when the system is becoming stable, and allowing a limited number of applications prevents this issue.

4.3 Combined Control Algorithm

The classification selection output is a set of controls $R \subset A$. The controls that make the sequences of this set include tripping generators in set Γ_θ, shedding load at bus locations in set Γ_ω, and inserting shunt capacitance as locations in set Γ_V. Next an optimization algorithm searches each of these possible control actions, along with the no control option, to find which sequence of controls has the lowest total cost.

The total cost consists of two components. The first is the cost of state deviation from target levels Eqn. 2.4.11. The second component of cost measures the impact of the controls, and is defined as $C_{control}$. These are adjusted depending on whether the no-control case is modeled as stable or instable. If stable, then the cost of controls is increased. If unstable, then the cost of issuing no controls is increased. Integer values are used as the cost for each control and the total control cost $C_{control}$ is their summation. Individual costs are shown in Table 4.3.1. For a given implementation the cost values might differ from the ones used here.

Table 4.3.1. Control costs for experimental verification.

Control Action	Base case is modeled stable	Base case is modeled unstable
No control action	1	4
Shunt capacitance	2	1
Load shedding	4	3
Generator tripping	3	2

The total cost includes both the effect of states and controls and the sequence of structures is selected to minimize this total cost, Eqn. 3.4.4. At each control iteration the reduced space of available controls R is recomputed. This adaptation of the reduced search space improves performance because it allows the space R to move within the space A according to the instantaneous conditions of the power system. There is a slight performance penalty for recomputing R at each iteration but it is relatively minor because a modeling over the finite horizon for the no-control case is necessary as part of the control selection process, independent of the control classification step. Therefore, the only penalty is ranking the costs and recalculating Eqn. 4.2.2, both of which are relatively minor compared to the rest of the control optimization steps.

It is always possible to reduce the size of control space A simply by allowing fewer controls. However, arbitrarily creating subset R provides no guarantees on the size of $R1$, which needs to be large, or the size of $R2$, $R3$, and $R4$ which need to be small. The benefit of the method described here is creation of space R that not only reduces the search space but also provides a set of controls which can meet the performance objectives.

4.4 Experimental Results

Verification of the approach is by comparing stabilizing control for the full admissible control space with the space restricted according to the algorithm in the previous sections. The same contingency is selected as was used for the experimental validation of Section 3.5. This is an outage on lines 21-22, 26-28, and 17-27. The severity of this contingency, with generators in two portions of the power system effected, provides a very challenging case for the classification method to stabilize. A 10% random error is added to the model parameters to include the inevitable effect of model parameter inaccuracy. The delay interval t_U is set at 50 milliseconds and the modeling interval of prediction is set at three seconds. The model is 6^{th} order, including rotor angle, frequency, internal voltage, machine power, and rotor voltage, as described in Chapter 3. When this same contingency was previously tested the admissible control space included removing nine generators, the load at nine bus sets, and inserting capacitance at one bus. The result is $N_A = 19$ individual structural changes considered by the controller. From Fig. 4.1.2, the search space size is $\mathcal{N}_A = 362$ and this is compared later to the computational demands of the classification method.

As part of the experimental testing, it is important to verify that region R with empty $R1$ is not found. Another possible problem is if region $R1$ is much smaller than region $R2$ and because of this a control in region $R2$ is modeled to have a cost smaller than the best cost in region $R1$. It is the finite window nature of control selection, selecting individual controls at each iteration from R, along with the iterative nature of the classification method that provides this possibility. Then, even though a valid control is available that meets the cost objective, a control in region $R2$ is selected which results in a higher cost control applied to the system.

Such a finding does not mean that the classification method has failed. It simply identifies the tradeoff between better computational performance and better cost-based control selection.

The fault occurs at time 1 second and continues until 1.45 seconds, at which time all three lines trip. The initial iteration of the control algorithm is at 1.5 seconds, or, 50 milliseconds after the lines are cleared. Ranking the cost calculation of Eqn. 3.4.1 for $C'_\theta(j)$ results in $\Gamma_{rank,\theta} = \{6,7,4,3,2,5,10,8,9\}$, which makes the highest cost generator $J = 6$. Then, based on the frequency difference $\left|\omega_{j,W} - \omega_{J,W}\right|$ the set of generators available for removal is $\Gamma_\theta = \{6,7\}$. One set of loads is allowed for removal and is found by finding the bus associated with largest value of $C'_\omega(j)$. The result is that set $\{21, 23,24\}$ is selected. For shunt compensation, the highest cost according to $C'_V(j)$ is for bus #16. A total of $N_R = 4$ individual control actions are then included in the admissible control set. Two for generation shedding, one for the bus shedding set, and one for shunt capacitance. From Fig. 4.1.2 the result is a total of $\mathcal{N}_R = 21$ sequences are considered by the optimal control algorithm. Comparing this to the $\mathcal{N}_A = 362$ required for the full admissible control space indicates a nearly 95% reduction in the size of the space the controller searches. This directly reduces computational demands and decreases the response time of the controller.

The controller then receives time-synchronized state measurements as initial values and applies the model, Eqn. 3.2.1 through Eqn. 3.2.7 for each of the admissible control sequences. State deviation costs are computed by summation of Eqn. 3.4.1, 3.4.2, and 3.4.3. The control costs follow Table. 4.3.1 and then selection is with Eqn. 3.4.4. The result is that removal of generation #6 is selected as the first control and applied at 1.55 seconds. So far the

control matches what was selected for the full admissible control space example in Section 3.5.

At the next iteration, a similar process for selecting the admissible control space follows and in this case $\Gamma_\theta = \{9\}$, $\Gamma_\omega = \{21, 23, 24\}$, and $\Gamma_V = \{26\}$. It is interesting that generator #9 is included in the admissible control space and generator #7 is not included. This is because the control application of removing generator #6 has resulted in generator #7 moving towards equilibrium. The controller then selects a capacitance change as the control action and the result is applied to the power system at time 1.65 seconds.

After waiting for the system to settle, the controller receives new time-synchronized state measurements and iterates for a third time. In this case there is no control available that provides a better result than doing nothing. Therefore, the controller does not apply any controls. Further iterations result in the same outcome and the process effectively terminates. It is interesting that the controller with full set of admissible controls applied a load shedding operation for the third iteration and this difference as compared to the result for the reduced set of admissible controls is now investigated. Table 4.4.1 provides the list of $\Gamma_{rank,\theta}$ at each iteration, along with the frequency difference $\left|\omega_{j,W} - \omega_{J,W}\right|$.

Table 4.4.1. Frequency difference at each generator, ranked by cost.

Iteration #1 (1.5 seconds)		Iteration #2 (1.6 seconds)		Iteration #3 (1.7 seconds)	
Generator	$\lvert\omega_{j,W} - \omega_{J,W}\rvert$, milliHertz	Generator	$\lvert\omega_{j,W} - \omega_{J,W}\rvert$, milliHertz	Generator	$\lvert\omega_{j,W} - \omega_{J,W}\rvert$, milliHertz
6	0	9	0	9	0
7	14	7	1370	7	330
4	3616	8	1656	6	441
3	3552	5	1824	5	534
2	3554	4	1819	2	516
5	3636	10	1768	3	551
10	3560	3	1809	8	195
8	3573	2	1819	10	272
9	3706	NA			

The results in Table 4.4.1 show that the frequency difference between the machines declines with each iteration. This is a result of the control actions. It also shows that after removing generator #6, the next generator showing the highest cost $C'_{\theta}(j)$ is generator #9. The cost metric $C'_{\omega}(j)$ follows a similar pattern, where cost associated with generator #9 becomes largest after the initial control action. This is the reason why the third iteration does not shed load, because the load shedding options in R change to those associated with generator #9, and it is becoming more stable. The load that was shed for the full admissible control space is not included in R at the third iteration.

Figure 4.4.1 shows the result after application of controls and includes time spans for pre-fault, fault-on, post fault, and control actions. As seen by observing the rotor angles and voltages, the system is stabilized. However, since the best load shedding option was not included in the reduced admissible control space R, the frequency declines significantly. In an actual implementation under frequency load shedding schemes would arrest the decline by shedding load according to their characteristics. This scenario fits with the original problem definition of the dissertation. Existing power system controls are allowed to act. The purpose of the optimal controller is to select a structure that minimizes a defined metric of cost and allows existing governors, automatic voltage regulators, and even system wide protection such as automatic load shedding to act according to their design.

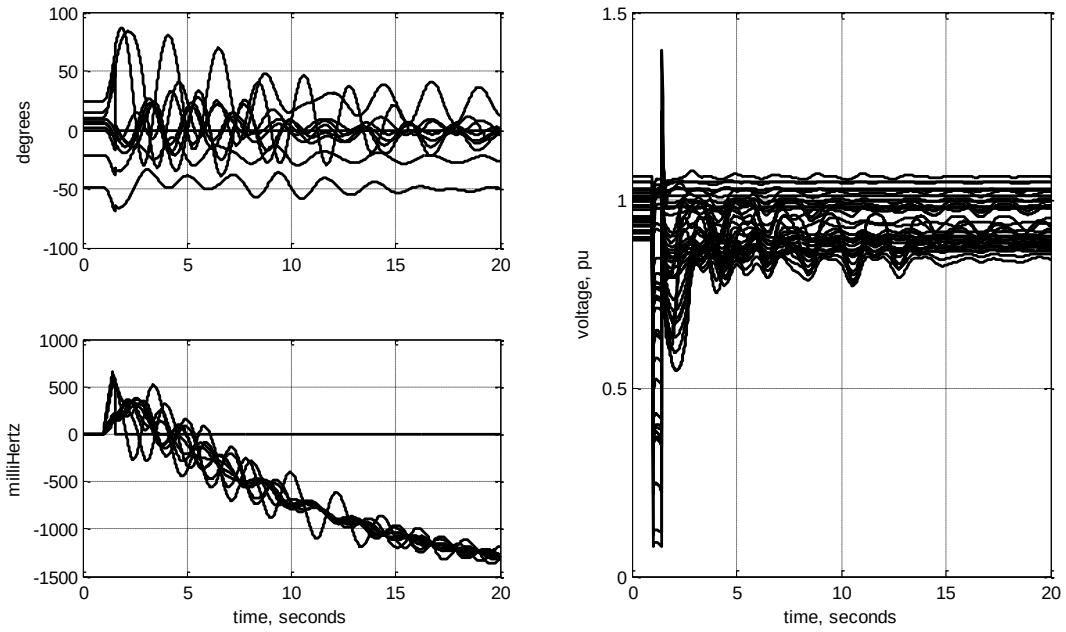

Figure 4.4.1. Response for stabilized conditions.

In addition to this detailed example, the classification method is applied to all of the 67 three line outage contingency cases as defined in Chapter 3. In all cases the system is brought to a stable equilibrium point. Also, unlike the detailed example just considered, in almost every other case the set of controls selected by the controller acting on the reduced set of admissible controls are identical to those selected when the controller acts on the full set of admissible controls. The previous example was selected for detailed analysis because of the difficulty it presents to the controller. It demonstrates the power of the optimal based structural change controller in stabilizing even a case that involves three line outages and two geographically separated sets of generators becoming unstable compared to the rest of the system. It also demonstrates that when the full algorithm is modified to reduce computational demands it sometimes leads to a less optimal control selection. But the system is stabilized by the controller.

5.0 MODEL-FREE CONTROLLER

A model of the system is required for selecting structural change controls with the previously described algorithms. A key advantage of the model is that it provides a systematic framework for selecting the best control. It also provides the ability for prediction and therefore gives additional time to determine and act with the controls. Disadvantages include the possibility of model inaccuracies and the large computational burden. Another issue is the practical difficulty of building and maintaining models. Errors in the model are mitigated by the iterative, feedback nature of the previous approaches. The computational burden is improved by adaptively partitioning the admissible control space, developed as the classification algorithm.

This chapter designs a controller that further reduces the number of calculations required. No model is required, only historical measurements. The design method is through a heuristic approach. The controller does not have the ability to correct the same wide range of contingencies as the previous two designs. However, a portion of the cost metric is maintained therefore the controller still does well with many high order contingencies. The result is a system that is simple to implement and demonstrates reasonably good performance, both in terms of its ability to stabilize difficult contingencies and to select suitable controls.

5.1 Algorithm Timeline

A timeline of the approach is shown in Fig. 5.1.1. An initial fault on the system is at time t_F and then existing protection and controls remove one or more assets at t_T. Time-synchronized state measurements are collected into a buffer while the system evolves along a post-fault trajectory. When sufficient data is collected, the algorithm initiates. The historical buffer is in place of prediction. The buffer of measured data means that a model is not required. Instead, however, the controller must wait for a sufficient number of measurements in the buffer before selecting a control decision.

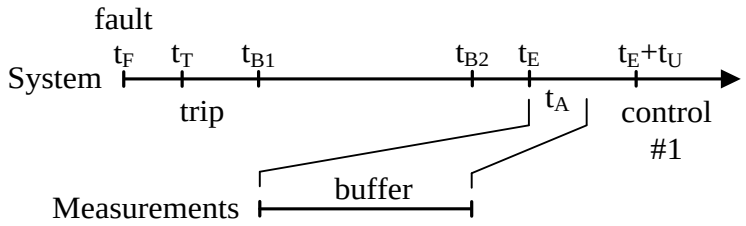

Figure 5.1.1. Timeline for the historical classification control algorithm.

Data collection begins at time t_{B1} and continues until time t_{B2}. The delay from t_T until t_{B1} allows for communication latencies. The data received is time-stamped voltage magnitudes $V_{j,i}$ and time-stamped rotor angle measurements $\theta_{j,i}$, where j is an index of the individual devices in the system and i indexes time. The voltage magnitudes are synchrophasor values from phasor measurement units (PMU). Data is received at a fixed rate of f_{nom} samples per second and therefore i is a notational short form indicating time at $i\left(1/f_{nom}\right)$.

The length of historical data received is set by the time difference $t_{B2} - t_{B1}$. The buffer length in units of samples is set by the update rate. A small buffer is necessary for transient stability control. This ensures a fast response time. However, to accurately assess the stability of the system, and to select appropriate controls, a large buffer is needed. Later in the experimental section it is shown that a buffer duration on the order of hundreds of milliseconds is adequate. This results in the size of the buffer, L_B, in range of 3 to 15 samples.

$$L_B = f_{nom}(t_{B2} - t_{B1}) \qquad 5.1.1$$

One of the challenges of the historical approach is the necessity of a small window. The previous controllers applied models and prediction. Modeling the system behavior in advance allows a longer window over which to select controls. This is because waiting for a sufficient buffered set of measurements is not required. Only a measurement at a single instant of time is needed to initialize the models. However, the model with prediction introduces computation time into the control actions. So, there is an inherent tradeoff between the model and the model-free approaches. The response time of the model approach is constrained by waiting for the computations to complete and the response time of the model-free approach is constrained by waiting for measurements.

The controller executes at time t_E after a receiving a complete set of buffered measurements. A time duration of t_A seconds is allowed for algorithm processing. Then, if a control action is required, it is sent to the machines or loads and takes effect at time $t_E + t_U$. Once a control is sent then determination of the sufficiency of the control is by waiting until the system settles and then collecting another buffer of measurements, as shown in Fig. 5.1.2.

If a control was not required after the first iteration, then the second iteration executes at time $t_E + t_S$, instead of waiting for a complete new buffer of data. In this case the old data is removed from the buffer and new data is added in a first-in-first-out (FIFO) manner.

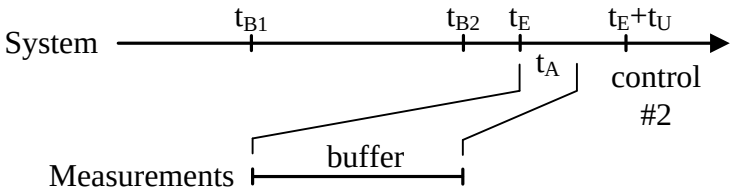

Figure 5.1.2. Second iteration of historical classification.

5.2 Algorithm Design

The historical classification algorithm consists of two stages. First, stability is assessed. This determines the need for controls. Second, controls are selected. The need for a separate stability assessment stage is new to the historical classification controller. It is required because no model or prediction is available to aid in control selection. Therefore, controls are issued only subsequent to determining that the system is becoming unstable. This is in contrast to the previous two controllers which could use a model to determine the consequences of issuing a control. The optimization algorithm inherently rejected any controls that made the system response worse and therefore avoided applying controls when the system was stable.

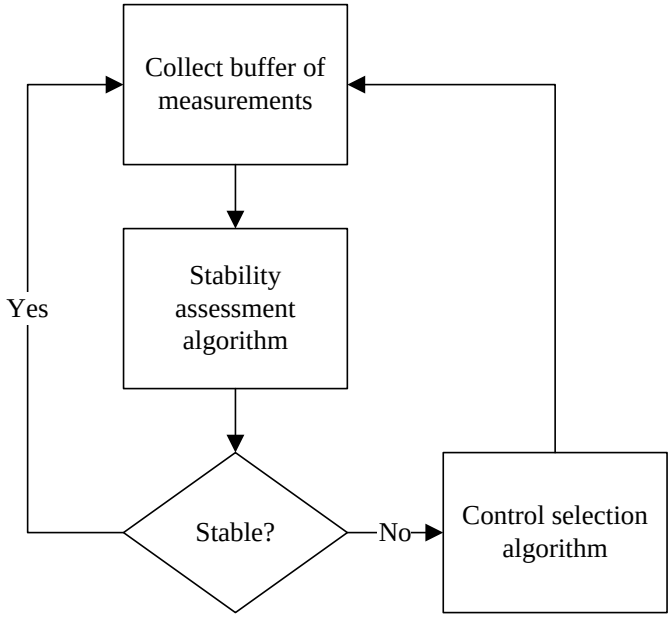

Figure 5.2.1. Historical classification flow diagram.

Both stages of the historical classification control algorithm utilize similar cost metrics, although with different reference values. A cost is calculated following the method of Section 2.4. Each state value in the window of length W is from a measurement, not from a modeled output. The result is that the summations run from the most recent time to the start of the buffered state measurements.

$$C'_{\theta}(j,w) = \frac{1}{W^2}\sum_{i=w+W}^{w} \frac{\left(\tilde{\theta}_{j,i} - \bar{\tilde{\theta}}_j\right)^2}{\pi^2} \tag{5.2.1}$$

$$C'_{\omega}(j,w) = \frac{1}{W^2}\sum_{i=w+W}^{w} \frac{\left(\omega_{j,i} - \omega_{ref}\right)^2}{\omega_{limit}^2} \tag{5.2.2}$$

$$C'_V(j,w) = \frac{1}{W^2}\sum_{i=w+W}^{w} \frac{\left(V_{j,i} - V_{ref,j}\right)^2}{V_{max}^2} \qquad 5.2.3$$

Stability Assessment Algorithm (SAA)

At time t_E the controller has a set of buffered time-synchronized measurements and computes the performance metrics $C'_\theta(j,w)$, $C'_\omega(j,w)$, and $C'_V(j,w)$. Stability is assessed by first summing the metrics, Eqn. 5.2.4. For stability assessment, the reference frequency ω_{ref} in Eqn. 5.2.2 is set to the average frequency over the window. The voltage reference, $V_{ref,j}$ in Eqn. 5.2.3 is set to the equilibrium voltage values for the first iteration. If any control actions are necessary, then subsequent iterations use the average voltage over the buffer. This is because the stability assessment algorithm does not have a model available and the initial equilibrium values become less relevant once the structure of the system has changed.

$$G(w) = \sum_{j=0}^{M-1}\{C'_\theta(j,w) + C'_\omega(j,w)\} + \sum_{j=0}^{N-1} C'_V(j,w) \qquad 5.2.4$$

Initially, it might seem that comparing Eqn. 5.2.4 with a threshold can detect instability. A large combined performance metric implies all measured states have deviated significantly from their target values. This is an indication of instability. However, it is not robust to depend on a fixed value. Calculating a value depends on the system configuration and it changes with control actions. The value also depends on power flows, which can

change, as well as pre-fault state values. It is difficult to find a threshold that is simultaneously secure against falsely declaring instability and dependable to correctly identify conditions that lead to instability.

A better solution is monitoring changes in the metric Eqn. 5.2.4 over time. This approach, through a numerical derivative, is given by Eqn. 5.2.5. When the power system response is headed towards stability, then it seems reasonable that $G(w)$ decreases with time. This is because angles, frequencies, and voltages move towards mean-square reference values. When the response of the system is moving towards instability, then it is likely that $G(w)$ increases with time because the monitored cost values tend to diverge. In Eqn. 5.2.5, $G(w-1)$ is the cost metric derived from data at a sample $1/f_{nom}$ in time previous to the present sample.

$$D(w) = G(w) - G(w-1) \tag{5.2.5}$$

The differentiation is qualified for security before application as a predictor as instability. Fig. 5.2.2 shows the set of calculations, including qualification.

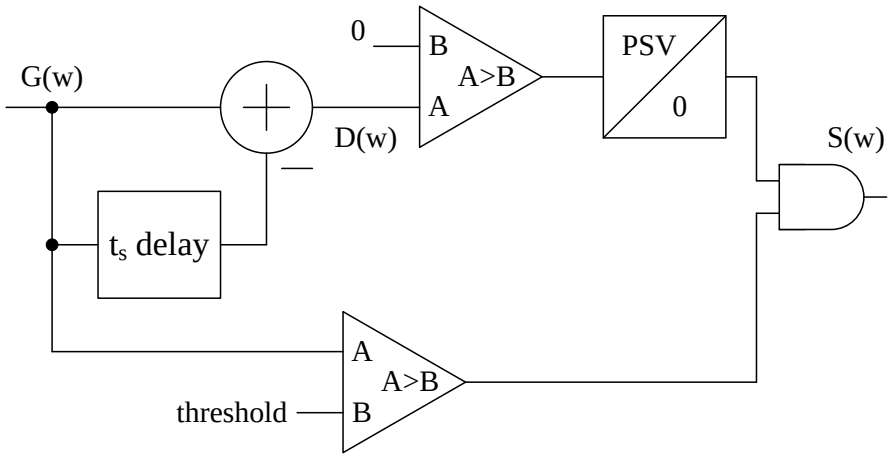

Figure 5.2.2. Stability assessment algorithm logic diagram.

In Fig. 5.2.2, $G(w)$ is numerically differentiated, with a time step corresponding to the controller execution interval, $t_s = {}^{1}/_{f_{nom}}$. The difference value $D(w)$ is compared against zero. When $D(w)$ is positive, this means that the performance metric has increased. For security and rejection of spurious noise in the differentiation process a sequence of consistent increases is enforced by the pick-up timer. The setting value (PSV) determines the required number of repeated positive values. The pick-up timer output provides an assessment that the system is becoming unstable and a control is required. A specific value of PSV is provided in the experimental section.

The threshold as shown in Fig. 5.2.2 does not require a precise value because it is only serving as a qualification to avoid noise from differentiation for small metrics. Security against excessive control actions, control instability, is possible by progressively increasing the threshold value after each control action is taken. The system is assessed as becoming

unstable, and requiring a control, when $S(w)$ asserts. Here is a summary of the stability assessment algorithm. The algorithm executes at each time interval t_s.

1. Calculate the rotor angle performance metric $C'_\theta(j,w)$ for each machine $j = 0, \ldots, M-1$ according to Eqn. 5.2.1.
2. Calculate the rotor angle performance metric $C'_\omega(j,w)$ for each machine $j = 0, \ldots, M-1$ according to Eqn. 5.2.2.
3. Calculate the rotor angle performance metric $C'_V(j,w)$ for each machine $j = 0, \ldots, N-1$ according to Eqn. 5.2.3.
4. Compute $G(w)$ with Eqn. 5.2.4.
5. Compute the difference, Eqn. 5.2.5.
6. Determine if the difference is larger than zero. If so, keep track of the number of times this difference exceeds zero in a row.
7. If the difference exceeds zero for PSV intervals in a row and if $G(w)$ exceeds a coarse threshold, then assert a flag S indicating an unstable condition.

Control Selection Algorithm

The control selection algorithm builds on the theory developed for the classification control method. The classification method was previously applied to reduce the search space for optimal control selection. Now, without a model, there is no further information available to help determine which of the controls in the subset to select. Instead, apply all controls in the reduced space R to the system. The resulting controls might be suboptimal because no additional refinement is added to the algorithm to distinguish between these controls.

However, the classification algorithm has selected controls based on a cost metric applied to the historical buffer data. Therefore, the results of this approach are reasonably successful at stabilizing the system at acceptable cost, as shown later in the experimental section.

The control selection algorithm proceeds by first ranking the costs $C'_\theta(j,w)$ in order from largest to smallest. These costs are based on a buffer of historical data, instead of a predicted set of data. The frequency of the most recent measurement is then used to select a subset of the generators associated with these costs. Define this set of frequencies as $\omega_{j,W}$, where $j \in \{1,\dots,M\}$, and also define the frequency in this set corresponding to the machine with largest $C'_\theta(j,w)$ as $\omega_{J,W}$. Then, apply Eqn. 4.2.2 to calculate the criteria frequency $\Delta\omega_{crit}$. The subset of generators Γ_θ selected for tripping are selected by traversing the costs $C'_\theta(j,w)$ starting at the largest value, and continuing until a machine is found with the most recent frequency measurement such that $\left|\omega_{j,W} - \omega_{J,W}\right| > \Delta\omega_{crit}$. Measurement sensor noise is easily reduced by filtering the last few frequency values to compute a derived value for $\omega_{j,W}$.

Frequency is calculated from $\omega = {d\theta}/{dt}$. Then, rank the costs $C'_\omega(j,w)$ in order from highest to lowest. Because the entire space R is selected as the controls at each iteration, it is beneficial to reduce the size of R more significantly than was needed for the classification method. Previously, the main disadvantage of large space R was requiring extra computations. Now, however, an excessive number of controls in space R can result in control instability. So, the selection algorithm is modified towards biasing to a smaller R. Specifically, it is preferred to remove as little load as possible. Governors at the generators will pick up some of

the imbalance. Therefore, only a specified fraction of the power difference is corrected by the action of load shedding.

Selection of loads to shed proceeds as follows. First, start with bus j associated with the largest value of $C'_{\omega}(j,w)$. Calculate the power of the associated load using measured values received from synchrophasor measurements. This power value is defined as P_j. Compare this power to a specified fraction γ of the total shed generation power P_T. If the amount of load power shed meets or exceeds this total, then finish. The set of loads selected for removal is complete. Otherwise, continue consideration of further loads, progressing from those associated with larger performance metric $C'_{\omega}(j,w)$ values to smaller values until the total shed load power matches or exceeds the fractional amount of generation removed. In calculating $C'_{\omega}(j,w)$ for load shedding ω_{ref} is set to the nominal frequency. This forces the control algorithm to select controls such that the frequency returns to its nominal range. The fraction γ is a tunable parameter that allows trading the amount of load shed against the amount of state deviation tolerable. Setting this fraction closer to unity means more load shedding is allowed. A smaller fraction sheds lesser load and requires governors on other generators, as well as spinning reserve, to pick up the imbalance.

A variety of methods are available to associate loads with generators. The algorithm nicely adapts to specific utility practices. If certain loads near a generator are unavailable for shedding then simply do not include them in the association with that generator. Alternatively, in some cases contractual relationships make a load available for shedding. In this case include it. For this work, loads are selected by traversing the power system network away from the generator until the first load is found.

5.3 Experimental Results

Detailed Example

Suitability of the measurement based approach is validated using the same contingency as was analyzed in the previous two chapters. The unstable response of the system without controls was shown in Fig. 3.5.2. This contingency is particularly severe and provides a difficult test of the algorithms. The buffer length for this experiment is set to six samples. The delay for buffering is therefore 100 milliseconds. The sample rate is $f_{nom} = 60$. Referring back to Fig. 5.1.1, $t_{B2} - t_{B1} = 100$ milliseconds.

There is an inherent tradeoff in buffer size selection. Making the buffer longer provides more information for stability assessment and control selection. However, with a longer buffer this means a longer time until controls are applied. If the system is becoming unstable then waiting to apply controls gives the system more time to evolve away from any nearby stability regions.

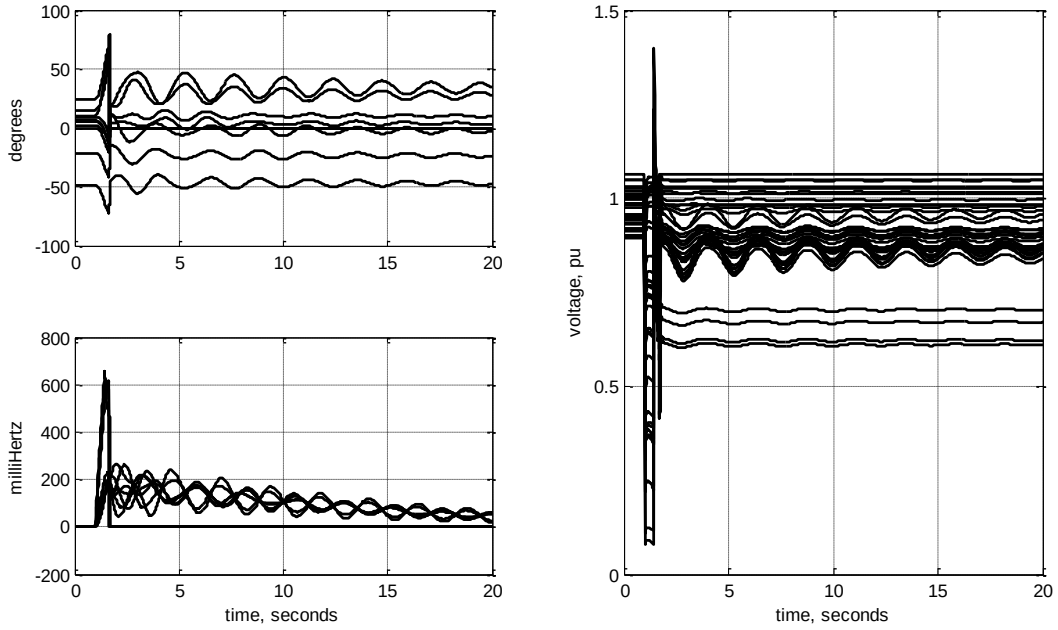

Figure 5.3.1. Results after stabilization for historical method.

Figure 5.3.1 shows the result after the historical classification method applies the controls it has selected. The control algorithm has successfully stabilized the system. A detailed analysis is as follows. Start with the fault at $t_F = 1$ second. The lines trip after the fault condition at time $t_T = 1.450$ milliseconds. Once the trip condition is detected the controller is notified and begins collecting and buffering the time-synchronized measurements. The controller first executes once the buffer contains six samples. The pick-up timer PSV is set for two sequential samples. At time $t = 1.583$ milliseconds the output of Fig. 5.2.1, S, asserts to indicate an unstable condition. Once the system is assessed as unstable, the control selection algorithm executes. This is at time $t_E = 1.583$ milliseconds. Table 5.3.1 shows the order of $C'_\theta(j, w)$

cost metrics, from largest to smallest. Also shown are frequency differences from the machine with the largest metric. The criteria frequency, $2\pi\Delta\omega_{crit}$ is 215 milliHertz.

Table 5.3.1 Metrics for generator tripping selection.

Generator	$2\pi\left\|\omega_{j,W} - \omega_{J,W}\right\|$, milliHertz
6	0
7	9
9	78
3	430
2	424
8	424
4	411
10	394
5	358

Devices selected for removal are generator #6, generator #7, and generator #9. Similarly, the computation for load shedding results in removal of loads at bus #16, bus #20, bus #21, bus #23, bus #29, and bus #32. The load shedding parameter γ was set to 0.75. The value t_U was set to 50 milliseconds to allow for communication latencies and actuation delays.

Compare this set of controls to the optimal controller applied over the full admissible control space, Table 3.5.1. The full controller, with model for control selection, removed one generator, inserted one series capacitor, and shed load at three buses. The historical controller, with a model-free selection, removed three generators and shed load at six buses. So, the historical controller took a more expensive option. This is not unexpected since it did not explicitly consider the costs of the controls. However, the computational burden is much less and no model is required. Comparing the state trajectory performance between these two cases, Fig. 3.5.3 for the full controller and Fig. 5.3.1 for the historical controller, shows they are similar for rotor angle and frequency. However, the voltage performance is worse for the historical controller. Again, this is a result of the less computationally demanding, but also less optimal control selection.

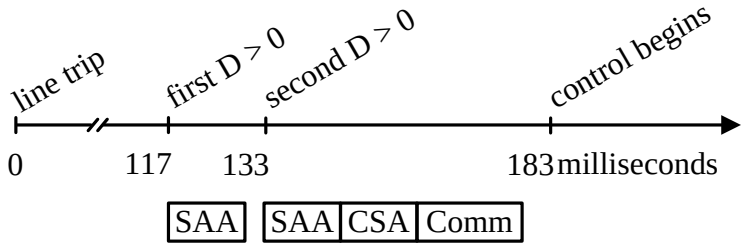

Figure 5.3.2. Sequence of events for the example.

Figure 5.3.2 shows a timeline of the actions for this test case, referenced to the time of the line trip. In this figure, SAA represents the stability assessment algorithm, CSA represents the control selection algorithm, and Comm indicates communication delay. While the stability assessment algorithm estimates that the system is stable, the control selection algorithm does not run and controls are not selected. Once instability is detected, then the control selection

algorithm executes. Cost of controls is implicitly included by using a criteria frequency and set of rotor angle metrics to keep the number of generators removed as small as possible. Similarly, for load shedding, frequency metrics enable finding locations where load shedding has the greatest impact on restoring balance. This reduces the amount of load required for removal.

Comparison Against 67 Cases

Additional verification of the model free algorithm is through testing against the same set of 67 test cases as were used for the full controller. Results show that the method is able to suitably assess stability and select controls that stabilize the system. Three of the cases, however, proved problematic. In these cases too many controls were applied and the system was disassembled fairly completely. This is an example of control instability, Eqn. 2.4.15. The results of these tests indicate that there are certain contingencies for which the historical classification controller is not suitable, as expected.

Comparison With Different Buffer Lengths

The previous examples operated with a buffer length of 100 milliseconds, which means six samples were available for computing the performance metrics, assessing stability, and selecting the controls. It might seem that a shorter buffer could provide a faster response, or, alternatively, a longer buffer could provide more accurate assessments. Perhaps one or the other might provide a better control response. To investigate these possibilities the detailed example was retested with a short 50 millisecond and a long 250 millisecond buffer length. The short buffer has a total of 3 measurements and the long buffer a total of 15 measurements

for calculating the performance metrics. Experimental results show that the generators selected for removal by the control algorithm are identical to those removed for the 100 millisecond buffer length case. However, when the buffer length increased to 500 milliseconds then performance degraded significantly, as shown in Fig. 5.3.3. This is because unstable conditions remain in the system longer, additional load shedding is required, and the system states swing over very wide ranges. The system is eventually stabilized. It is expected that other controls in the system arrest the significant frequency decline. The result of these experiments shows that there is a fairly wide margin in selecting the buffer length and values in the range of 50 milliseconds to 200 milliseconds give good results, for the system under consideration. The relative insensitivity to the buffer length is due in part to the mean square error formulation of the performance metric calculations.

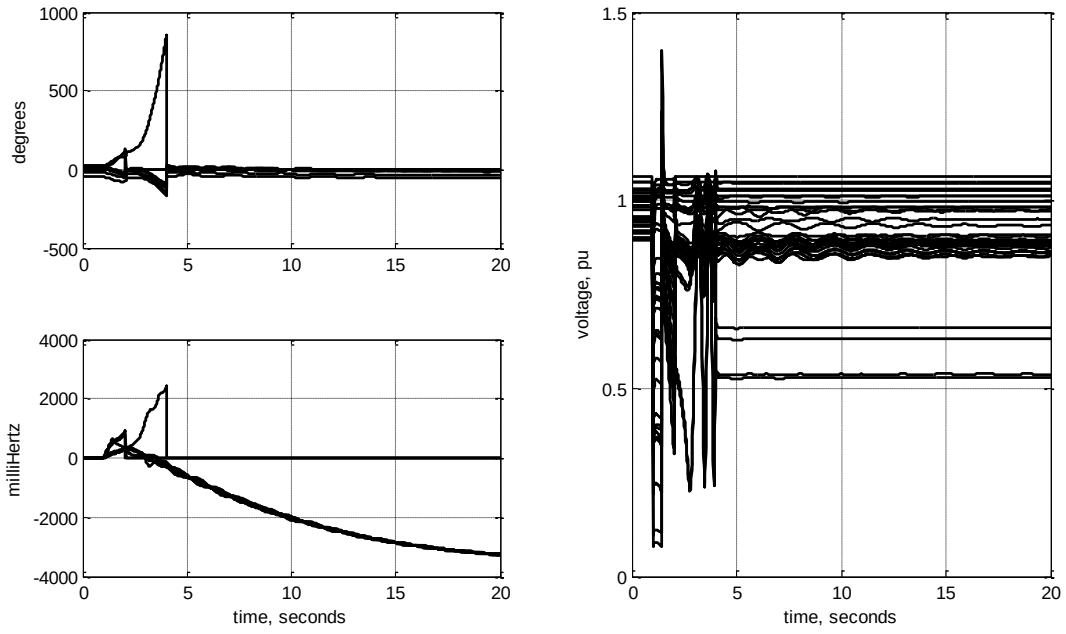

Figure 5.3.3. System response with a long buffer.

Security of Stability Assessment Algorithm

The control system developed here acts based on real-time system measurements and the actions are not planned in advance. It is important that these controls are restrained for cases when the system is stable. Key to such security is correct operation of the controller stability assessment algorithm. Verification, in part, is through considering a single stable line outage. The conditions are set with a 100 millisecond fault time, which results in a significant amount of acceleration to the rotors. The system oscillates severely but then settles to stability. When the control algorithm is enabled, the stability assessment logic determines that the system is moving towards stability. No controls are issued. The resulting rotor angles with the controller enabled are shown in Fig. 5.3.4.

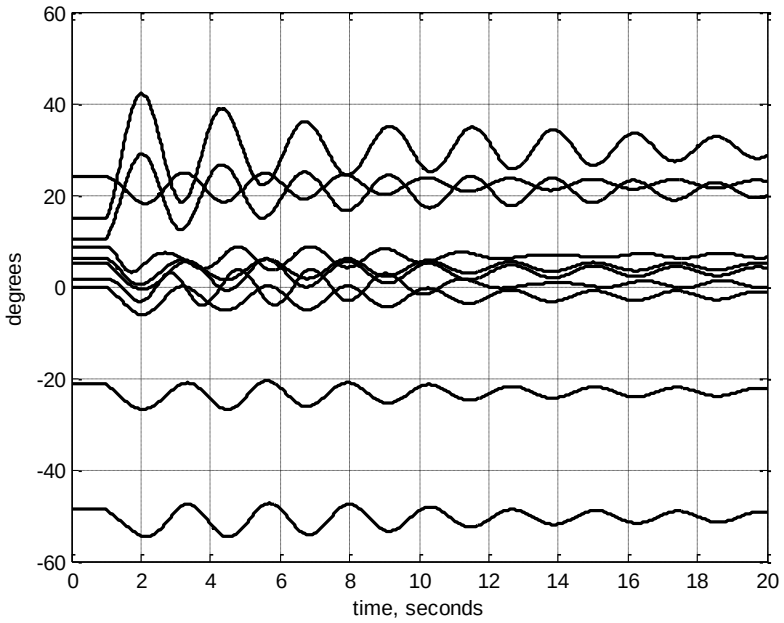

Figure 5.3.4. Rotor angles after disturbance without controls applied.

6.0 CONCLUSIONS

A methodology to design a control system that responds to rotor angle instability through stepped structural changes, including dimensional reduction, has been provided in this dissertation. After developing the methodology, two implementations are designed, analyzed, and tested. A third implementation applies the developed cost-metrics in a unique way towards a suboptimal but less computationally expensive approach.

Experimental results show many advantages of the approaches developed here including robustness to modeling errors, robustness to unexpected contingencies, and good performance in stabilizing a wide range of contingencies and initial conditions. The three implementations range from most to least complicated for implementation, giving opportunity for real-time implementation. The following summary of these methods helps in understanding their performance advantages and disadvantages.

Here are the processing steps for the unconstrained approach:

1. Measure the state of the power system using synchrophasors for the network state and time-synchronized measurements for the machine states.
2. Project the evolution of the system with an appropriate model for each control in A.
3. For each sequential combination of controls in admissible set A compute $C'_{\theta}(j,w)$, $C'_{\omega}(j,w)$, and $C'_{V}(j,w)$, and combine to create a cost of the state deviation from target trajectories, C_{state}.
4. Compute the controls costs $C_{control}$, based on T_{stab}

5. Select a sequence of structures from admissible control space A to minimize the total trajectory and control cost $\mathcal{J}$.
6. Apply the first control in the selected sequence to move the power system to a new structure.
7. Repeat.

Here are the processing steps for the classification method:

1. Follow the first two steps of the full method, except the prediction is only for the case without applying controls.
2. Build the sets Γ_θ, Γ_ω, and Γ_V. This becomes the reduced admissible set R.
3. Predict the evolution of the system for each control in R.
4. Compute the controls costs $C_{control}$, based on T_{stab}
5. Select a sequence of structures from admissible control space R to minimize the total trajectory and control cost $\mathcal{J}$.
6. Apply the first control in the selected sequence to the power system.
7. Repeat

The historical classification approach makes no predictions and requires no model. It monitors the present time-synchronized state, retains their history, and applies controls when the rate-of-change of a stability threshold is met.

1. Measure the state of the power system using synchrophasors for the network state and time-synchronized measurements for the machine states.
2. Compute $C'_\theta(j,w)$, $C'_\omega(j,w)$, and $C'_V(j,w)$ over the buffer of measurements.

3. Check if the rate of change of the state metric costs is positive for a certain length of time, if so, build the sets Γ_θ and Γ_ω.
4. Apply all of the controls in Γ_θ and Γ_ω.
5. Repeat.

The first method iteratively calculates costs based on a full admissible control set. The second method adaptively limits the admissible control set as a means to reduce computational complexity but retains the iterative cost selection method. The final method is model free and applies controls based only on a recent history of measurements.

The first method requires the largest computational demands and selects a sequence of controls with the lowest overall cost, including both the cost of state excursions as well as the cost of the controls. The second method reduces the admissible control space over which costs are computed and does so in a manner that does not significantly impact the selection of controls. Therefore, it has the advantage of both improving computational performance and selecting controls with a method that is optimal based. The third method requires a relatively modest amount of computation and can stabilize the system but makes no explicit guarantees about the cost of the controls or whether lower cost controls are available.

For minimum computation time, T_A of Fig. 3.1.3, the Eqn. 3.4.4 control selection is parallelizable. Simple test all structural sequences simultaneously in individual processing units or threads. Then, compare the resulting cost. Independence of computation is an advantage of the first two methods. A parallel approach is also possible for the third controller in calculating Eqn. 5.2.1, 5.2.2, and 5.2.3.

It is shown that the first two methods correct a wide range of contingencies. High order contingencies, while rare, can lead to wide area outages. Therefore, methods to react against such possibilities are beneficial. The third method cannot claim suitability for as many contingencies or classes of systems.

The development of these three methods provides an interesting means to understand tradeoffs between computation and optimization. As computing power, memory access speeds, and communication capabilities increase, the viability of the best performing algorithm increases. However, when such an approach is not possible, the analysis presented here demonstrates the effect of moving to sub-optimal, but more implementable approaches.

7.0 REFERENCES

[1] G. Constable and B. Somerville, *A Century of Innovation: Twenty Engineering Achievements That Transform Our Lives*, Joseph Henry Press, 2003.

[2] S. Wiggins, *Introduction to Applied Nonlinear Dynamical Systems and Chaos*, Springer, 2003.

[3] J. Guckenheimer and P. Holmes, *Nonlinear Oscillations, Dynamical Systems, and Bifurcations of Vector Fields*, Applied Mathematical Sciences 42, Springer, 1983.

[4] V. Venkatasubramanian, H. Schattler, J. Zaborszky, "A Taxonomy of the Dynamics of Large Differential-Algebraic Systems", *Proceedings of the IEEE*, vo. 83, no. 11, 1995, pp. 1530-1561.

[5] P. Kundur, J. Paserba, V. Ajjarapu, G. Andersson, A. Bose, C. Canizares, N. Hatziargyriou, D. Hill, A. Stankovic, C. Taylor, T. V. Cutsem, V. Vittal, "Definition and Classification of Power System Stability", *IEEE Trans. Power Systems*, vol. 19, no. 2, May 2004, pp. 1387.

[6] M. Vaiman, K. Bell, Y. Chen, B. Chowdhury, I. Dobson, P. Hines, M. Papic, S. Miller, P. Zhang, "Risk Assessment of Cascading Outages: Methodologies and Challenges", *IEEE Trans. On Power Systems*, vo. 27, no. 2, 2012, pp. 631 – 641.

[7] Q. Chen, Y. Lin, J.D. McCalley, "The Risk of High-order Transmission Contingencies", *IEEE Power Engineering Society General Meeting*, June 24 – 28, 2007, p. 1.

[8] A.G. Phadke, J.S. Thorp, K.J. Karimi, "State Estimation with Phasor Measurements," *IEEE Trans. Power Systems*, vol. PWRS-1, no. 1, February 1986.

[9] R. Zivanovic and C. Cairns, "Implementation of PMU Technology in State Estimation: An Overview," *proc. IEEE 4th AFRICON*, Sept. 24-27, 1996, vol. 2, pp. 1006-1011.

[10] M.S. Braasch, A.J. Van Dierendonck, "GPS Receiver Architectures and Measurements", *Proceedings of the IEEE*, vo. 87, no. 1, Jan. 1999.

[11] G. Benmouyal, E.O. Schweitzer, A. Guzman, "Synchronized Phasor Measurement in Protective Relays for Protection, Control, and Analysis of Electric Power Systems", *29th Annual Western Protective Relay Conference*, Spokane, Washington, October 22-24, 2002.

[12] SEL-421-4, -5 Relay Protection and Automation System Instruction Manual, Schweitzer Engineering Laboratories, Inc. February 14, 2012.

[13] E. O. Schweitzer, III, D. Whitehead, G. Zweigle, and K. Gubba Ravikumar, "Synchrophasor-Based Power System Protection and Control Applications," *36th Annual Western Protective Relay Conference*, Spokane, Washington, October 2009.

[14] Y. Chen, C. Zhang, Z. Hu, X. Wang, "A New Approach to Real Time Measurement of Power Angles of Generators at Different Locations for Stability Control," *IEEE Power Engineering Society Winter Meeting*, 2000.

[15] G. Zweigle, D. Finney, R. Moxley, "Adding Shaft Angle Measurement to Generator Protection and Monitoring", *Western Protective Relaying Conference, Spokane*, WA, Oct, 2012.

[16] P. Wang, W. Deng, Z. Qian, "Method for the Measurement of Rotor Voltage and Current of Power Generator", *IET Generation, Transmission, and Distribution*, vol. 4, issue 7, pp. 854 – 860, July 2010.

[17] D.E. Bakken, A. Bose, C.H. Hauser, D.E. Whitehead, G.C. Zweigle, "Smart Generation and Transmission with Coherent, Real-Time Data", *Proceedings of the IEEE*, vol. 99, issue 6, pp. 928 – 951, June 2011.

[18] V. Madani, D. Novosel, S. Horowitz, M. Adamiak, J. Amantegui, D. Karlsson, S. Imai, A. Apostolov, "IEEE PSRC Report on Global Industry Experiences with System Integrity Protection Schemes (SIPS)", *IEEE Trans. Power Delivery*, pp. 2143 – 2155, Oct. 2010.

[19] M. Sherwood, D. Hu and V. Venkatasubramanian, "Real-time Detection of Angle Instability Using Synchrophasors and Action Principle", *2007 iREP Symposium – Bulk Power System Dynamics and Control – VII*, August 2007, Charleston, SC.

[20] P. Kundur, *Power System Stability and Control*, New York: McGraw-Hill, 1994.

[21] C.W. Taylor, D. Erickson, K. Martin, R. Wilson, V.Venkatasubramanian, "WACS – Wide Area Stability and Voltage Control System: R&D and Online Demonstration," *Proceedings of the IEEE*, vol. 93, no. 5, May 2005.

[22] J.B. Rawlings, "Tutorial Overview of Model Predictive Control," *IEEE Control Systems Magazine*, June 2000, pp. 38 – 52.

[23] M. Larsson, D. Karlsson, "Coordinated System Protection Scheme Against Voltage Collapse Using Heuristic Search and Predictive Control," *IEEE Trans. Power Systems*, vol. 18, no. 3, Aug. 2003, pp. 1001 – 1006.

[24] M. Glavic, M. Hajian, W. Rosehart, T.V. Cutsem, "Receding-Horizon Multi-Step Optimization to Correct Nonviable or Unstable Transmission Voltages," *IEEE Trans. Power Systems*, 2011.

[25] L. Jin, R. Kumar, N. Elia, "Model Predictive Control-Based Real-Time Power System Protection Schemes," *IEEE Trans. Power Systems*, vol. 25, no. 2, May 2010, pp. 988 – 998.

[26] D. Ruiz-Vega, M. Pavella, "A Comprehensive Approach to Transient Stability Control: Part I – Near Optimal Preventive Control", *IEEE Trans. Power Systems*, vol. 18, no. 4, Nov. 2003, pp. 1446 – 1453.

[27] D. Ruiz-Vega, M. Pavella, "A Comprehensive Approach to Transient Stability Control: Part II – Open Loop Emergency Control", *IEEE Trans. Power Systems*, vol. 18, no. 4, Nov. 2003, pp. 1454 – 1460.

[28] M. Glavic, D. Ernst, D. Ruiz-Vega, L. Wehenkel, M. Pavella, "E-SIME – A Method for Transient Stability Closed-Loop Emergency Control: Achievements and Prospects," *2007 iREP Symposium – Bulk Power System Dynamics and Control – VII*, August 2007, Charleston, SC.

[29] Chih-Wen Liu, James S. Thorp, "New Methods for Computing Power System Dynamic Response for Real-Time Transient Stability Prediction," *IEEE Trans. Circuits and Systems*, vol. 47, no. 3, Mar. 2000, pp.324-337.

[30] A.D. Rajapakse, F. Gomez, K. Nanayakkara, P. A. Crossley, V. V. Terzija, V.V, "Rotor Angle Instability Prediction Using Post-Disturbance Voltage Trajectories", *IEEE Trans. Power Systems*, vol. 25, no. 2, pp. 947-956, May 2010.

[31] J. Xiao, X. Xie, H. Lu, J. Wu, Y. Han, "Power System Dynamic Security Assessment via Synchrophasor Monitoring", *Power System Technology 2004*, Nov. 21-24, pp. 930-935.

[32] B. Wu, O.P. Malik, "Multivariable Adaptive Control of Synchronous Machines in a Multimachine Power System," *IEEE Trans. Power Systems*, vol. 21, no. 4, Nov. 2006, pp. 1772 – 1781.

[33] W. Yao, L. Jiang, J.Y. Wen, S.J. Cheng, Q.H. Wu, "An Adaptive Wide-area Damping Controller Based on Generalized Predictive Control and Model Identification", *Power and Energy General Meeting*, July 26-30, 2009, pp. 1-7.

[34] D. E. Kirk, *Optimal Control Theory, An Introduction*, Dover Publications, Inc. 1998.

[35] T. L. Vincent, W. J. Grantham, *Nonlinear and Optimal Control*, New York: John Wiley & Sons, Inc., 1997.

[36] W. L. Brogan, *Modern Control Theory, 3rd Edition*, Prentice Hall, 1991.

[37] G. Zweigle and V. Venkatasubramanian, "Wide-area Optimal Control of Electric Power Systems with Application to Transient Stability for Higher Order Contingencies", *IEEE Trans. Power Systems*, 2013.

[38] G. Zweigle and V. Venkatasubramanian, "Model Prediction Based Transient Stability Control", *IEEE PES Conference and Exhibition*, 2012.

[39] G. Zweigle and V. Venkatasubramanian, "Methods for Mitigation of Rotor Angle Instability with Cost Based Control", *In preparation.*

[40] G. Zweigle and V. Venkatasubramanian, "Application of Time-Synchronized Rotor Angle Measurements to Wide-Area Stability Control", *In preparation.*

[41] S. H. Strogatz, *Nonlinear Dynamics and Chaos, Studies in Nonlinearity*, Westview Press, 1994.

[42] Report to the NERC Board of Trustees by the NERC Steering Group, "Technical Analysis of the August 14, 2003, Blackout: What Happened, Why, and What Did We Learn," July 13, 2004.

[43] L.E. Franks, *Signal Theory, Revised Edition*, Dowden and Culver, Inc., 1981.

[44] T. Yang, H. Sun, A. Bose, "Transition to a Two-Level Linear State Estimator – Part I: Architecture", *IEEE Trans. Power Systems*, vol. 26, no. 1, February 2011.

[45] Matlab User's Guide, MathWorks, 2012.

[46] Transient Security Assessment Tool User Manual, Powertech Labs, Inc. August 2011.

[47] C.W. Taylor, *Power System Voltage Stability*, Electric Power Research Institute Power System Engineering, 1993.